FATIGUE EVALUATION OF NANOCOMPOSITES AS LIGHTWEIGHT ELECTRONIC ENCLOSURES FOR SATELLITES' APPLICATIONS

THESIS

Javier Rodriguez, Captain, USAF

AFIT/GMS/ENY/09-M03

DEPARTMENT OF THE AIR FORCE
AIR UNIVERSITY

AIR FORCE INSTITUTE OF TECHNOLOGY

Wright-Patterson Air Force Base, Ohio

The views expressed in this thesis are those of the author and do not reflect the official policy or position of the United States Air Force, Department of Defense, or the United States Government.

AFIT/GMS/ENY/09-M03

FATIGUE EVALUATION OF NANOCOMPOSITES AS LIGHTWEIGHT ELECTRONIC ENCLOSURES FOR SATELLITES' APPLICATIONS

THESIS

Presented to the Faculty

Department of Aeronautics and Astronautics

Graduate School of Engineering and Management

Air Force Institute of Technology

Air University

Air Education and Training Command

In Partial Fulfillment of the Requirements for the

Degree of Master of Science (Materials Science)

Javier Rodriguez, BS

Captain, USAF

March 2009

AFIT/GMS/ENY/09-M03

FATIGUE EVALUATION OF NANOCOMPOSITES AS LIGHTWEIGHT ELECTRONIC ENCLOSURES FOR SATELLITES' APPLICATIONS

Javier Rodriguez, BS
Captain, USAF

Approved: Date:

/signed/ 4 March 09
Dr. Shankar Mall (Chairman)

/signed/ 4 March 09
Dr. Som Soni (Member)

/signed/ 4 March 09
Dr. Vinod Jain (Member)

Abstract

The United States Air Force is evaluating the use of nanocomposite materials for satellite structural applications. Exposure to the space environment requires protection from radiation and other harsh conditions. Existing composite materials don't provide the required level of electrical conduction and electromagnetic shielding, and requires the addition of metal shields in order to operate in space. The Materials and Manufacturing Directorate of the Air Force Research Laboratory (AFRL) in conjunction with the private sector have developed a composite material that promises to blend the attributes of nanocomposite structures with the electrical traits of metallic materials. The developed material is the M55J/RS3, a graphite fiber combined with polyisocyanate matrix space qualified material which has Nickel nanostrands™ embedded into the resin, to improve the electrical properties of the material.

In our research effort we investigated the changes in the electrical properties of the M55J/RS3 material while it was subjected to different cycles and cyclic stress levels (fatigue loading). Resistance & EMI measurements were taken before and after each fatigue load was applied in order to have initial values and to document changes in the resistance & EMI properties. All configurations consisted of a symmetric 8 plies layup of M55J/RS3 material with its fibers oriented at 0/90/45/-45 degrees. Three of the four configurations had nickel nanostrands™ layers, making the composite more conductive. The Control configuration is the configuration with no nickel nanostrands™. The remaining three configurations are based on the control configuration, but the location of the added nickel nanostrands™ varied among them. The Exterior configuration had the

nickel nanostrands™ on the outer plies of the laminate. The Midplane configuration had the nickel nanostrands™ in the middle part of the laminate, between the -45° plies and the Interlaminar had the nickel nanostrands™ between the 0° and 90° laminates and between the 45°and -45° laminates.

Analysis of the test data showed that after 2 million cycles at 60% (ultimate tensile strength (UTS) level the exterior configuration performed better keeping its conduction and EMI shielding of specimen. For higher stress levels the trend was similar regarding electrical properties, but the interlaminar configuration maintained its structural integrity longer than any other configuration during the 75%UTS level test. Overall, the exterior configuration had the best performance having the lowest initial and final resistance values for all stress levels. It also offered the highest initial and final EMI values for all stress levels. Inspection of fractured specimens showed that the 90° plies failed first. In all cases it was observed that delamination occurred between the 0° and 90° plies, near the free edge of the specimen. Matrix cracking and subsequent delamination between the 45° plies resulted in total failure of the specimens at 75% and 90% of the UTS level. Evaluations of tested specimens showed that nickel nanostrandsTM were undamaged during the test.

Acknowledgements

I would like to thank my wife for her caring and support during the last 18 months and throughout my entire time in the USAF. I would also like to thank my academic and thesis advisor Dr. Shankar Mall for his patience and advice. I would like to thank Dr. Max Alexander for his assistance with the EMI shielding and resistance measurements as well as the professors of the ENY department for their guidance throughout the program.

Javier Rodriguez, Captain, USAF

Table of Contents

Page

Abstract...iv

Acknowledgements...vi

Table of Contents...vii

List of Figures...x

List of Tables...xiv

List of Symbols and Acronyms...xv

I. Introduction...1

II. Background...7

2.1 The Space Environment...7

2.2 M55J/RS3 Composite Materials...9

2.3 EMI & Electrical Properties...11

2.4 Previous Research Effort at AFIT...16

2.5 Fatigue Testing...17

2.6 M55J/RS3 Failure Mechanisms...20

2.7 Summary...21

III. Method of Experimentation...23

3.1 Introduction...23

3.2 Specimen Preparation...23

3.3 Fatigue Testing Equipment and Procedures...23

3.4 MPT Procedure Editor...27

Page

3.5 EMI Test Equipment and Procedures…….…….....28

3.5.1 Settings Procedure.....….....28

3.5.2 Calibration……..…….…..28

3.6 Resistance Testing……...…….…...31

3.7 Test Plan Summary…….....32

IV. Analysis and Results……..34

4.1 Introduction…….……34

4.2 Resistance Measurements……35

4.2.1 Resistance for 70% UTS Stress Level…….....35

4.2.2 Resistance for 60% UTS Stress Level…….....38

4.2.3 Resistance for 75% UTS Stress Level.....41

4.2.4 Resistance for 90% UTS Stress Level…….....45

4.3 EMI Shielding.…….....48

4.3.1 EMI for 60% UTS Stress Level….……...49

4.3.2 EMI for 75% UTS Stress Level…….……...52

4.3.3 EMI for 90% UTS Stress Level……54

4.4 Fatigue Testing - Failure Mechanisms ……57

4.4.1 Fatigue Testing - 60%UTS……...58

4.4.2 Fatigue Testing - 75%UTS……...62

4.4.3 Fatigue Testing - 90%UTS……...71

4.5 Number of Cycles vs. Stress Levels….……...73

Page

V. Conclusions and Recommendations……..75

5.1 Summary……..……75

5.2 Conclusions……...……...76

5.3 Recommendations for Future Work…….……78

Appendix A. MTS Testing Sequence……..79

Appendix B. Additional SEM Photos……82

Bibliography.....85

Vita……87

List of Figures

Figure Page

1. GPS Satellite [20].…….....1

2. Nanostrands™ in Polymer Matrix [1]……..…….3

3. Laminate lay-up [19]...……...5

4. a. Fiber Reinforced Composite [19..…….....9

4. b. Laminate Construction [19]…….....9

5. a. 100 Nanometer Diameter Nickel Nanostrands™[1]……..……..12

5. b. Compressed Nanostrands™ Lattice [1]...…….....12

6. Volume Resistivity of Spray Epoxy and Elastomer Paints [1]……...13

7. 625,000 Volt Discharge without Ni Nanostrands™ [1].....14

8. Controlled Electrostatic Discharge with 5% volume Ni Nanostrands™ [1].…….....14

9. Electromagnetic Shielding Properties [1]…….……...15

10. Relative Structural Efficiency of Aircraft Materials [19]..……..……..18

11. Tension-Tension with Applied Stress [19]...……...…….....19

12. Damages in Fiber-Reinforced Composites [3].…….....20

13. M55J/RS-3 Testing Specimen…...…….…….……..…23

14. MTS 810 System.…….…….25

15. Station Manager Program…..…….…….....26

16. MPT Procedure Editor Test Sequence…….....27

17. Red Mark on Specimen.…….…….…….……..30

18. EMI Test Set-Up..……..30

Figure Page

19. Extech Milliohm Meter…….....31

20. M55J/RS-3 Composite Configurations…….....34

21. Resistance Comparison for 70% UTS Level.....37

22. a. Resistance Comparison for 60% UTS Level.....40

22. b. Initial and Final Values for 60% UTS Level…….……40

23. Normalized Resistance Values for 60% UTS Level……..41

24. a. Resistance Comparison for 75% UTS Level……..…..…...……..…..……44

24. b. Initial and Final Values for 75% UTS Level……....……45

25. Normalized Resistance Results for 75% UTS Level.……..…..…….....45

26. a. Resistance Comparison for 90% UTS Level……..…..…...……..…..……47

26. b. Initial and Final Values for 90% UTS Level……....……48

27. Normalized Resistance Results for 90% UTS Level.……..…..…….....48

28. a. EMI Comparison for 60% UTS Level…….....51

28. b. Initial and Final EMI Values for 60% UTS Level.....51

29. Normalized EMI Values for 60% UTS Level……51

30. a. EMI Comparison for 75% UTS Level……..……..…..…...……..…..……53

30. b. Initial and Final EMI Values for 75% UTS Level……....……54

31. Normalized EMI Results for 75% UTS Level.……..…..…….....54

32. a. EMI Comparison for 90% UTS Level……..……..…..…...……..…..……56

32. b. Initial and Final EMI Values for 90% UTS Level……....……56

33. Normalized EMI Results for 90% UTS Level……...……..…..…….....57

34. Delamination.……..……..……..……..……...……57

Figure Page

35. 60% UTS Test Specimens…….58

36. 60% UTS Control Specimen ……..……..…..……..……59

37. 60% UTS Control Specimen ……..……..…..……..……59

38. 60% UTS Exterior Specimen ……..……..……..……60

39. 60% UTS Exterior Specimen ……..……..……..……60

40. 60% UTS Interlaminar Specimen……..……61

41. 60% UTS Interlaminar Specimen……..……61

42. 60% UTS Midplane Specimen……..……..……62

43. 60% UTS Midplane Specimen……..……..……62

44. 75% UTS Control Specimen.……..……..…..……..……63

45. 75% UTS Control Specimen.……..……..…..……..……63

46. 75% UTS Exterior Specimen.……..……..……..……64

47. 75% UTS Exterior Specimen.……..……..……..……64

48. a. SEM-75% UTS Exterior Specimen.……..……..…...65

48. b. SEM-75% UTS Exterior Specimen.……..……..…...65

49. 75% UTS Interlaminar Specimen….……..……...66

50. SEM-75% UTS Interlaminar Specimen....……..……...67

51. SEM-75% UTS Interlaminar Specimen....……..……...68

52. SEM-75% UTS Interlaminar Specimen....……..……...68

53. 75% UTS Midplane Specimen....……..…….69

54. a. SEM-75% UTS Midplane Specimen....……..……70

54.b .SEM-75% UTS Midplane Specimen...……..……..70

Figure Page

55. 90% UTS Control Specimen....…….…….....71

56. 90% UTS Midplane Specimen..…….…….72

57. 90% UTS Interlaminar Specimen..…….……72

58. 90% UTS Exterior Specimen.....…….……73

59. Number of Cycles vs. Stress Levels……74

60. SEM-75% UTS Exterior Specimen…….82

61. SEM-75% UTS Interlaminar Specimen……..83

62. SEM-75% UTS Midplane Specimen……...84

List of Tables

Table Page

1. Specimens' UTS Values……32

2. Tested Specimens. …….…….....33

3. Resistance for 70% UTS Level……...…….……..…….....35

4. Resistance for 60% UTS Level……...…….……..…….....38

5. Resistance for 75% UTS Level……...…….……..…….....42

6. Resistance for 90% UTS Level……..…….……..…….....46

7. EMI for 60% UTS Level……...…….……..…….....49

8. EMI for 75% UTS Level……...…….……..…….....52

9. EMI for 90% UTS Level……...……..…….……..……...55

10. Number of Cycles vs. Stress Levels……74

List of Symbols and Acronyms

AFIT	Air Force Institute of Technology
AFRL	Air Force Research Laboratory
GSM	Grams per Square Meter
σ	Stress
EMI	Electromagnetic Interference
ESD	Electrostatic Discharge
NS	Nickel Nanostrands™
Ω	Ohm
OM	Optical Microscope
SEM	Scanning Electron Microscope
USAF	United States Air Force
UTS	Ultimate Tensile Strength

FATIGUE EVALUATION OF NANOCOMPOSITES AS LIGHTWEIGHT ELECTRONIC ENCLOSURES FOR SATELLITES' APPLICATIONS

I. Introduction

Space is a unique environment that offers a myriad of opportunities for the exploitation of new and existing technologies. Numerous satellite applications are in use today and will continue growing in the future. Many services such as television, radio, telephone, GPS, and internet and can be received from a satellite directly to our homes or current location. Decades ago it was inconceivable for an ordinary citizen to think that it could be possible to have access to those services in remote areas. Satellite systems such as the GPS satellite shown in Figure 1 make this possible.

Figure 1. GPS Satellite

The United States Air Force (USAF) recognizes space as a crucial area on our nation's defense. New satellites are following the same trends of aircraft systems by increasing the use of composite materials to have a more effective system. Today, more than ever space superiority is critical to ensure and maintain America's safety and the leading edge in space operations. The space environment offers the capability to provide surveillance, communication, navigation, missile-warning, tracking and intelligence of thousands of objects, and the medium to conduct defensive and offensive counterspace operations and space environment assessments.

There are many factors that influence the material selection of a spacecraft. For example, high launching costs makes the system's weight a major factor for concern. Weight reductions can be achieved by using composite material instead of heavier alternatives such as metallic materials. Saved money could later be invested in better equipment and technology to improve the efficiency and reliability of the system. Spacecraft systems confront harsh conditions while in space which includes exposure to gases, dust, debris, radiation, cosmic rays, extreme temperatures, and electromagnetic waves in the form of X-Rays, UV Rays, visible light, infrared, radio waves and microwaves. These factors and others like out gassing phenomena are a major concern when selecting a material for space applications.

Metallic materials, like aluminum are commonly used because of their light weight, and their capacity to conduct charges and dissipate heat. Composite materials intended to for space environment, are required to provide similar capabilities to the materials being replaced. A USAF initiative to find more efficient, reliable, durable and electrically conductive substitutes is the study of the M55J/RS3 fiber reinforced

composite with Nickel Nanostrands™. The Materials and Manufacturing Directorate of the Air Force Research Laboratory worked in conjunction with Metal Matrix Composites of Utah to develop the M55J/RS3 fiber reinforced composite with nickel nanostrands™. Figure 2 shows a cross section view of the developed nickel nanostrands™ dispersed in a polymer matrix.

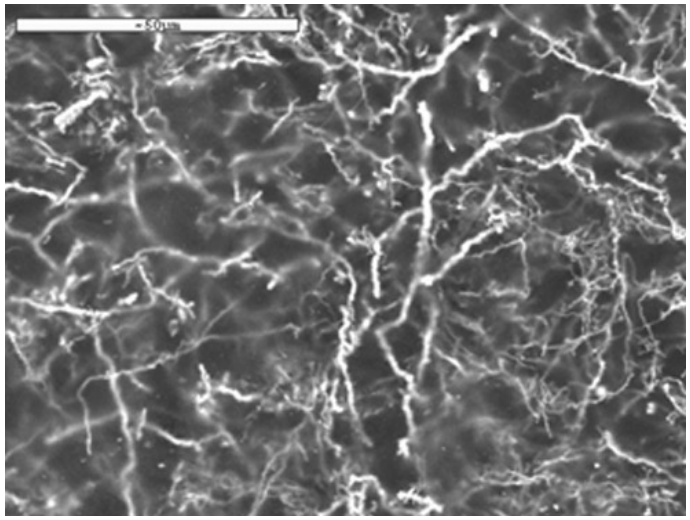

Figure 2. Nickel Nanostrands™ in a Polymer Matrix.

Fiber reinforced organic matrices offers an increase in the strength to weight ratio of the system, but are non conductive. Some of the ways to provide the electrical conduction to the composite are the insertion of metal foil, meshes or the use of metal based paint. These methods are not very efficient in making and keeping the composite highly conductive during its time in space, and for this reason other methods such as the insertion of metallic particles in the matrix of the material are being studied. Nickel material is conductive, magnetic and corrosion resistant. The inclusion of the Nickel Nanostrands™ into the composite's matrix provides the required electrical conduction and Electromagnetic Interference shielding.

Previous work done at the Air Force Institute of Technology (AFIT) by Captain Benjamin T. Harder on the space certified M55J/RS3 material included the evaluation of its structural and electrical properties before and after monotonic tension loads were applied up to fracture. Specimens were also exposed to a simulated space environment after which its structural and electrical properties were evaluated, before and after monotonic tension loads were applied. Tests results showed that the Ultimate Tensile Strength (UTS) and the Young's modulus (mechanical properties) did not change after exposure to the space environment. Evaluation of electrical properties showed that specimens that contained nickel nanostrands™ offered better EMI protection than the control specimen. Captain Harder's research effort was concentrated in applying monotonic tension loads up to fracture, but it is known that a system's stress level won't have to be near the material's ultimate strength to cause total failure. Fatigue fracture can cause the material to fail due to repeated loading.

The purpose of this study is to investigate the changes in the electrical properties of the M55J/RS3 material while being subjected to different cyclic stress levels. To examine the fatigue effects, we applied a cyclic load to 4 different configurations of the M55J/RS3 composite material and evaluated their behavior before and after each set of cycles. Three of the 4 configurations had nickel nanostrands™ layers added to improve the electrical properties of the material. The first configuration was the Control configuration, and consisted of a symmetric 8 plies layup of M55J/RS3 composite material with its fibers oriented at 0/90/45/-45 degrees and a fiber volume fraction (V_f), of 0.717.

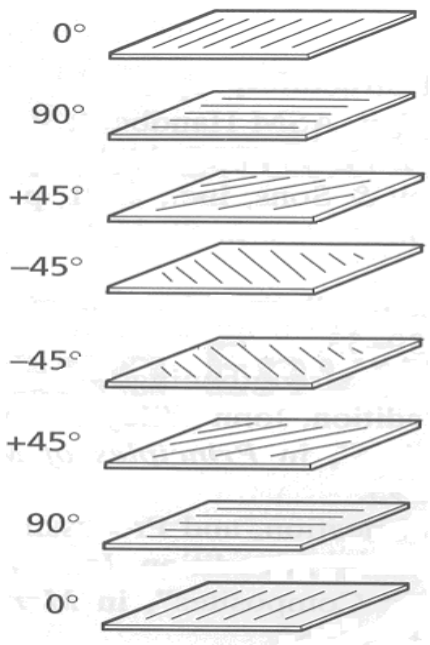

Figure 3. Laminate Lay-up.

The second configuration was the Exterior configuration, based on the control configuration, but with the addition of nickel nanostrands™ on the top and bottom part of the laminate. This configuration had100 grams per square meter (GSM) of nickel nanostrands on the top surface, and 100 GMS on the bottom surface. The third configuration was the Midplane configuration, based on the control configuration, but the addition of 200 grams per square meter (GSM) of nickel nanostrands™ in the middle part of the laminate, between the -45° plies. The 4th configuration was the Interlaminar configuration, also based on the control configuration with the addition of 50 GMS of nickel nanostrands™ between the 0° and 90°laminates and between the 45° and -45° laminates.

We were able to compare and see the differences in the electrical properties for the 4 different configurations of our composite material by using the Extech Milliohm

Meter to measure resistance, and The Agilent Technologies PNA Series Network Analyzer to measure EMI changes. Measurements were taken before and after each set of cyclic loads were applied. The cyclic load was applied using the MTS 810 servohydraulic testing machine. The specimens were initially tested at the 70% UTS stress level to become familiar with the procedure and to get a preliminary idea on the changes and the tendency for each configuration after applying cyclic loads. The specimen were later tested at a lower 60%UTS and higher levels of 75% UTS and 90% UTS.

The study of nickel nanostrands^{TM} is still relatively new. In the following chapters we will provide background information, methodology used, results of the fatigue testing, and analysis done on the 4 different M55J/RS3 composite configurations.

II. Background

2.1 The Space Environment

The space environment is a harsh surrounding for any spacecraft. The Sun is mostly responsible as it is the source for many particles and waves in space. Radiation, cosmic rays, and electromagnetic waves in the form of X-Rays, Gamma Rays, UV Rays, visible light, infrared, radio waves and microwaves are most of the Sun's energy contributions to space. The difference among the emitted electromagnetic waves is their wave length, but all have an electrical and magnetic component. They are created when an electrically charged particle oscillates or accelerates. The emitted energy from the sun flows in a continuous steady way, but at some point it can come in bursts.

Solar wind is another sun's energy contribution to space. It consists of a stream of particles composed of electrons, protons, and alpha particles that flows outward from the sun. Exposure to solar wind is equivalent to being exposed to low level of radioactive material. Solar flares are also released when energy wrapped in a magnetic field cannot contain itself anymore. This release results in mass ejections that reach very high speeds. These traveling particles are known as cosmic rays. There are also many other contributors such as radiation and the Van Allen Belts that can cause heat transfer problems for satellites'operations.

Radiation is defined as the transfer of energy from place to place by means of electromagnetic waves [5]. Radiation and electromagnetic interference affecting satellites includes electric and magnetic fields. These fields can induce current in circuit elements, damaging or altering the function and operation of components, potentially causing

failure of the system. Effects of radiation in organic materials include material's degradation and formation of new compounds due to the breaking of chemical bonds.

Space debris left behind by passing comets or left over after the solar system was formed, can also affect the structural integrity of satellites. The impact of a small piece of debris traveling at high speed could cause sufficient damage to alter the proper functioning of the system. Space environment extreme temperatures are also responsible for more problematic conditions such as outgassing phenomena and cold welding. Outgassing phenomena occurs when a material is placed in a very low atmospheric pressure such as a vacuum environment, and when subjected to heat some of the material's constituents are evaporated causing contamination of the vacuum. Due to the importance of satellite applications, low-outgassing materials must be specified in order to prevent a material's evaporation in space environments. Otherwise, any outgas in space could create instability of the system, especially if it has to record or measure sensitive data. Cold welding phenomena could occur when two similar metal surfaces come in contact under vacuum conditions. The two pieces will strongly adhere to one another causing the fusion of the materials.

Due to all these conditions and challenges it is important to perform a good evaluation process on possible material solutions because the properties and parameters of composites will determine the performance of the satellite. The M55J/RS3 testing process will contribute to the analysis and evaluation effort to ensure composite's compliance with the conditions of the environment.

2.2 M55J/RS3 Composite Material

The commercial and military aerospace industry have benefitted from the developing composite technology by being able to replace primary and secondary structural components, improving construction techniques, reducing the number of parts needed for construction, and lowering their costs. Composite materials are composed of two or more distinct phases. Typically one phase acts as the reinforcement (fiber) of the other phase (matrix) as shown in Figure 4. The purpose of the matrix is to keep the fibers together, which will be carrying the great majority of the applied loads. The goal is to make a combination that produces the most efficient composite material for the particular design and application. The M55J/RS3 composite was manufactured by bonding a series of plies together forming a laminate, with a repeated pattern of angles between plies. The composite consisted of a symmetric 8 plies layup of M55J/RS3 material with its fibers oriented at 0/90/45/-45 degrees. This arrangement allows the fibers in the principal load direction to carry most of the load, and the fibers aligned at other angles to reinforce the composite and carry any other type of loads different than the axial loads.

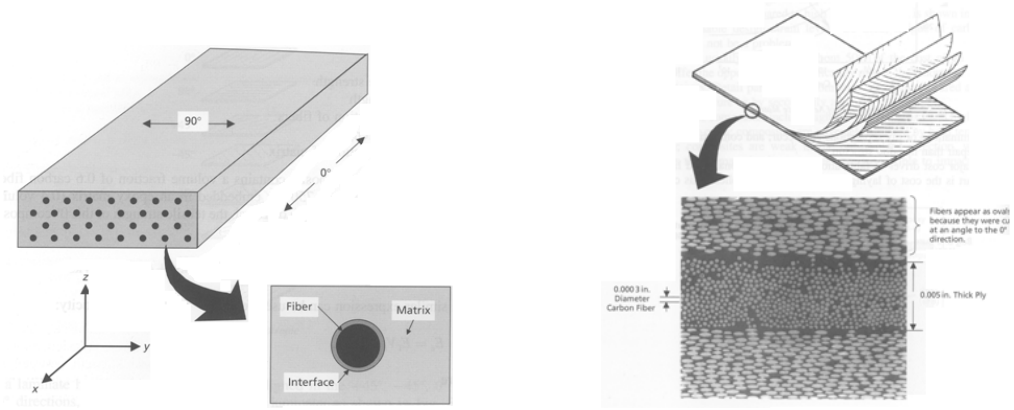

(a) (b)

Figure 4. (a) Fiber Reinforced Composite (b) Laminate Construction

The most common type of reinforcement fibers are continuous fibers. In the M55J/RS3 composite, graphite fibers provide the reinforcement in the material. The graphite fibers are all oriented in the same direction to provide the maximum structural properties in the direction parallel to the fiber. Graphite fibers are widely used as reinforcement material thanks to its extreme thin diameter. In general, graphite fibers have low density, low coefficient of thermal expansion, and are conductive. When the M55J fibers are embedded in the RS-3 matrix the result is a stronger, stiffer and tougher material.They also have great fatigue resistance, but low impact resistance, are brittle, and when comes in contact with aluminum may develop galvanic corrosion. The graphite fiber's alignment makes the composite material very strong for its size providing a high strength-to-weight ratio; however they lack the excellent electrical properties of a metal. The RS-3 resin is a modified 350 Fahrenheit degree cure polyisocyanate resin, designed to provide a tough material with a good high temperature/wet performance. This combination of M55J fibers and RS3 polyisocyonate resin has been used for many commercial and aerospace applications. Cyanate ester resins are associated with space applications because of their very low dielectric properties, extremely low moisture uptake, low outgassing, resistance to microcracking, and temperature resistance enough to withstand the extreme temperature changes in space.

With the addition of nickel nanostrands™ (nano-structured filamentary form) into the M55J/RS-3, the electrical properties such as conduction and electromagnetic shielding are improved. Only a small volume fraction of nanostrands™ are required to improve a material's conduction. The increase in the conduction is affected by the diameter, length, and orientation of the nanostrands™. Nickel nanostrands™ are very

long sub-micron diameter filaments having ranging from 50 nm to 1000 nm, with lengths ranging from tens of microns to tens of millimeters. The fabrication process for the nickel nanostrands™ inserted in the M55J/RS-3 was the Low Temperature Atmospheric Pressure Chemical Vapour Deposition (LTAPCVD). In a Chemical Vapour Deposition (CVD) process a chemical reaction of elements results in a solid deposit onto another material. At the moment the LTAPCVD process is conducted in a laboratory environment, which limits its production rate.

2.3 EMI & Electrical Properties

In addition to the sun electromagnetic waves and particles, AC electrical circuits tend to radiate electromagnetic waves into the space surrounding their elements, which further adds to the need for EMI shielding. A good EMI material needs to have high electrical conduction in order to shield electric fields, and magnetic permeability to shield magnetic fields. Most common EMI shields are made of aluminum and tantalum, and are formed into structural housing with a sheet thickness ranging from 0.060 to 0.250 of an inch. Both are effective, but Tantalum has a higher shielding effectiveness for magnetic fields. The main disadvantage of these materials when compared to composites is their weight. Nickel nanostrands™ were added into the M55J/RS-3 to provide EMI shielding protection, and ESD protection while taking advantage of the weight savings. In the past a conductive material phase such as a surface film had to be added to the material in order to provide the electrical properties to the composite. With the inclusion of metallic nanostrands™, the addition of the conductive material phase won't be necessary because the conductive medium is embedded in the material. Nanostrands™ are sub-micron filamentary metals with diameter ranging from 50 to 500 nanometers, and about 10 to

1000 microns long. This conductive medium forms a fully interconnected three dimensional nano-lattice throughout the composite material. The Nickel nano-lattice is mixed and dispersed into the polymer while it is in the liquid phase. After a sheet is formed it is pressed to concentrate the nickel nanostrands™ and increase the conduction of the material. Metal Matrix Composites Company of Utah fabricated the M55J/RS-3 material with nickel nanostrands™ used in this study. Nanostrands™ can be fabricated as a continuous sheet or rod that after being formed it can be pressed to concentrate the nanostrands™ and increase the conductivity. The originally produced lattice has a volume fraction of 0.3 % and a volume conductivity of about 1 Siemen/cm whereas the nanostrand™ lattice that has been compressed to about 20% volume solid increases the conductivity to about 5000 Siemens/cm, or 0.0002 ohmcm. Figure 5 shows the difference between the (a) originally produced nickel nanostrands™ and (b) nanostrand™ lattice that has been compressed.

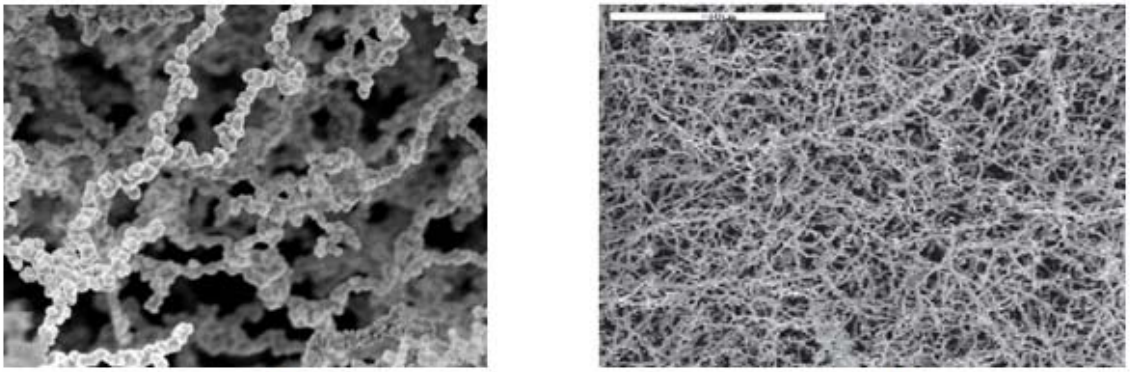

Figure 5. (a)100 Nanometer Diameter Nickel Nanostrands™ (b) Nanostrand lattice that has been compressed to about 20% volume solid

The insertion of nickel nanostrands™ into the M55J/RS-3 extends the electronic capabilities of the composite. With only small amounts of nanostrands™ an improvement

on the shielding properties can be experienced. With the addition of more nanostrands™ (conductive material) the composite will continue to reduce its resistance. Polymers with resistivity of about 102 ohm-cm and below are considered conductive for applications, with resistivity of about 100 or less are considered highly conductive. Resins with infiltrated nanostrands™ lattice exhibits excellent levels of conductivity on the order of 10^{-2} at very low volume fractions, and approached 10^{-4} at higher fractions [1]. Nanostrands™ can provide metal-like shielding capability in a wide variety of formats, such as paints, veils, gaskets, and composites. Figure 6 shows that small amounts of nanostrands™ added to 2 mediums, in this case an epoxy spray paint and a spray applied polyurethane elastomer, will cause an improvement on the conduction of the material. It also shows that nanostrands™ incorporation into different materials may result in different levels of conductivity.

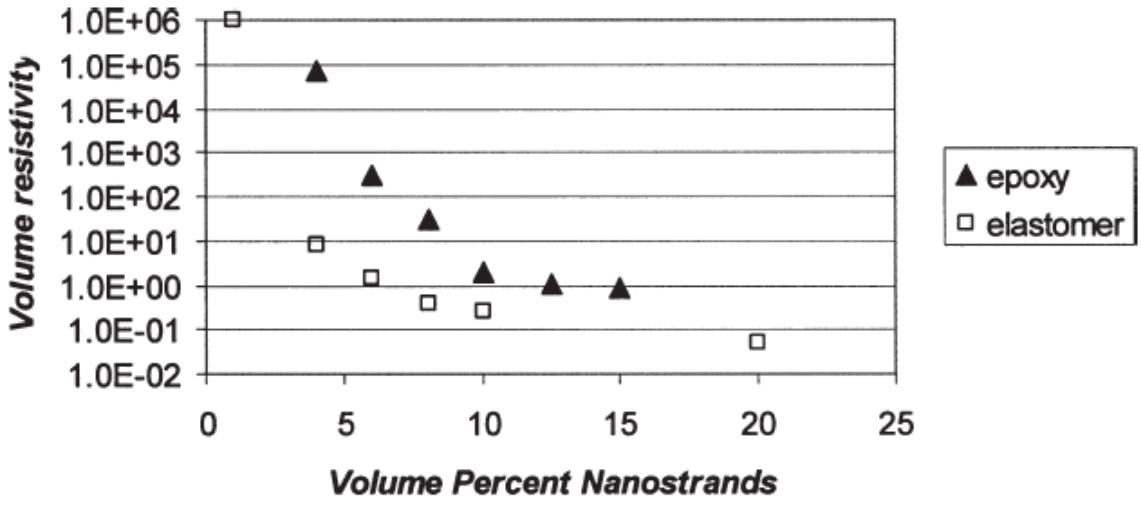

Figure 6. Volume Resistance of Spray Epoxy and Elastomer Paints

As mentioned previously, another contribution of the nickel nanostrands™ to the composite material is the electrostatic discharge protection. Tests performed by Metal

Matrix Composites Company of Utah have shown that even in low concentrations nanostrands™ provided sufficient conductivity to stop a 625,000 volt discharge. Figure 7 shows how a high voltage discharge easily penetrated an elastomer impregnated polyester cloth. In Figure 8, the same specimen with 5% nanostrands™ added was able to protect itself thanks to the conductive path provided nickel nanostrands™'. The added nickel nanostrands™ on the M55J/RS3 material will be providing the needed electrostatic discharge protection for the safe employment of the composite in extreme environments.

Figure 7. 625,000 Volt Discharge without Ni Nanostrands™

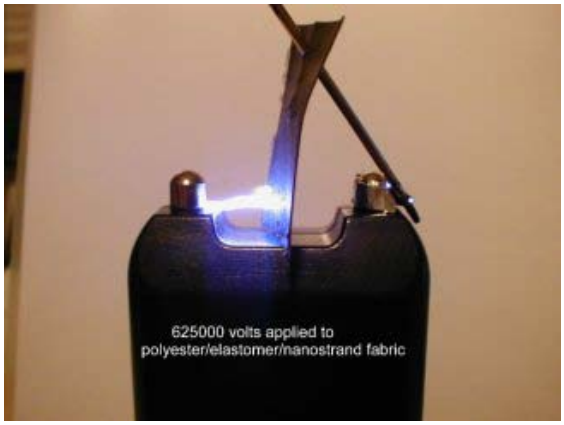

Figure 8. Controlled Electrostatic Discharge with 5% volume Ni Nanostrands™

Nanostrands™ have also proven to be effective in shielding electromagnetic radiation, a key property for space applications. The combination of electrical dc conduction, ferromagnetism, and nanostructured geometry, provides a high surface area and multiple angles of reflection and absorption making possible a highly effective EMI shield across a wide bandwidth. An EMI level of 60 dB is considered acceptable, and with the addition of nanostrands™ higher EMI levels can be reached. Added nickel nanostrands™shows how only a few mils of a nanostrand composite film provided an effective EMI shield across a wide bandwidth. Also, added nickel nanostrands™ different to other shielding materials, increased EMI protection at lower frequencies.

Figure 9 shows that for frequencies between 8 to 12 GHZ the performance of nickel nanostrandsTM was around the 60 dB EMI level providing the required electromagnetic shielding properties.

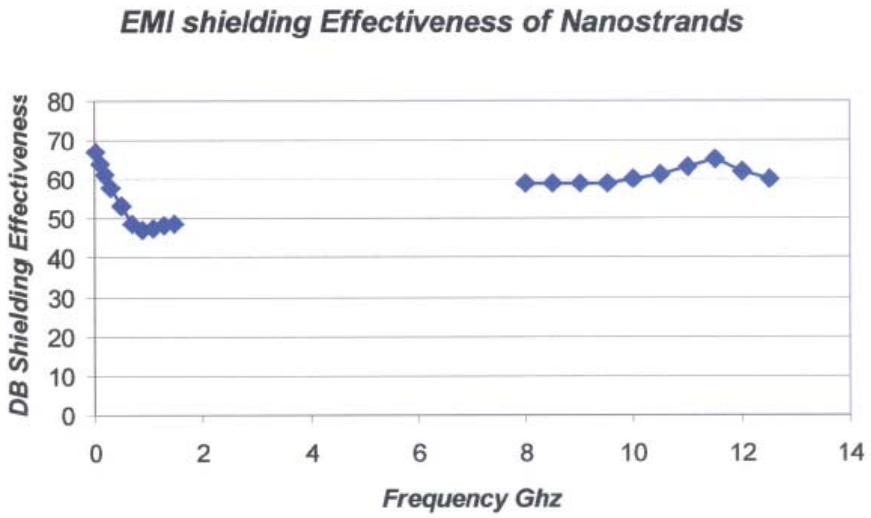

Figure 9. Electromagnetic Shielding Properties

2.4 Previous Research Effort at AFIT

Previous work done at AFIT by Captain Harder on the M55J/RS3 included specimens resistance measurements and EMI shielding tests under monotonic tension at different UTS levels, and specimens exposure to a simulated space environment. Four composite configurations of the M55J/RS-3 were tested in the previous effort (i.e. control, exterior, midplane and interlaminar). In order to establish baseline values, EMI shielding and resistance measurements were taken for each specimen before monotonic tension testing began. Monotonic tension was applied at different UTS levels to observe changes in their EMI shielding and resistance properties after each load increase, all the way up to fracture. The goal was to determine the tensile loading conditions effect on EMI shielding protection and resistance. Also, to know if the space environment affected the mechanical properties of the material, specimens were exposed to a representative five year space environment.

Analysis of the resistance measurement data showed that exterior specimens had the best performance. The exterior specimen's resistance remained almost constant while the interlaminar and mid-plane specimen's resistance steadily increases after each set of load was applied. Results showed that exterior specimens carried the current directly across the external surfaces protecting the material from charge buildup and successive ESD. EMI shielding was practically constant throughout the tensile loading conditions up to failure. The exterior specimens provided better EMI protection, and its EMI capability was 25% greater than the control specimen. The exterior specimens also provided better ESD protection, 11% greater than the control specimen.

Analysis of the space environment data showed that the specimens' UTS and Young's modulus did not change after exposure to the space environment. This was an indication that the nickel nanostrands™ provided protection from the interaction with charged particles. The EMI shielding protection decreased for all specimens, but specimens with nickel nanostrands™ still provided adequate EMI shielding protection. Failure mechanisms were the same for all 4 composite configurations. Damaged started in the 90° plies, causing delamination between the 90° and 0° plies leading to transverse matrix cracking. Propagation of damaged caused delamination between the 45° and -45° plies resulting in shear failure. Inspection of specimens showed that nickel nanostrands™ layers were not damaged and were providing protection up to fracture.

2.5 Fatigue Testing

In order for a material application to be successful, it first has to undergo an extensive analysis and evaluation process. During this time engineers try to determine all the possible scenarios that the new system will encounter and possible factors that could influence or affect its performance. The purpose of the evaluation process is to ensure the structural integrity of the design, and to minimize the risk of mission failure. In the space environment the material will be exposed to radiation, charged particles, debris, extreme temperatures and electromagnetic interference. A composite material in this environment needs to have a lot of the electrical characteristics of metals in order to be effective. For that reason a good material selection process is fundamental to ensure the proper performance of the system. The material selected must be able to overcome, sustain, and take into consideration all the applicable scenarios in order to be successful, and to

accomplish the mission for what it was built. Fatigue testing is one of the evaluation processes that help to assess the material's capacity of being durable and effective.

There are many ways for a material to fail, fatigue fracture being one of the most common. Deformation failure is defined as a change in the physical dimensions or shape of a component that is sufficient for its function to be lost or impaired (Dowling, 2007: 2). In a fatigue fracture the material fails due to repeated loading. Stress levels don't have to be near the material's ultimate strength to cause total failure, a marked difference from tension testing where the material fails after the ultimate tension stress level has been reached. The cyclic loading will cause very small cracks to appear in the material even at very low stress levels, which later will grow up to a point causing complete failure of the material. Figure 10 shows fatigue vs. tension testing results for two metals and a composite material. In the case of aluminum and Titanium we can see that these materials failed due to fatigue at stress levels that were almost half the stress levels at which failure occurs due to tension load.

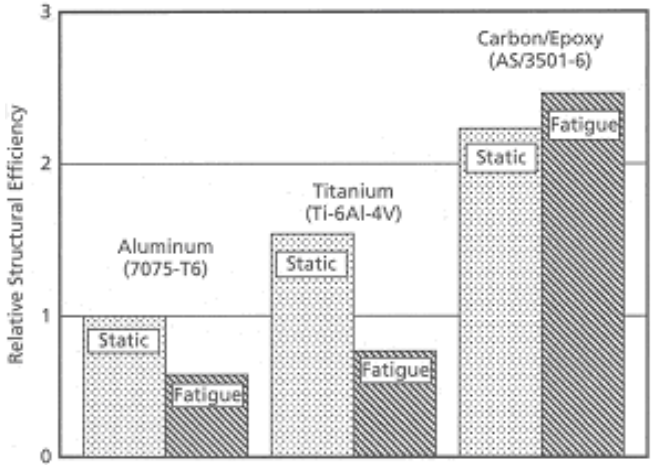

Figure 10. Relative Structural Efficiency of Aircraft Materials

During fatigue testing the material experiences a maximum stress and a minimum stress levels that are constant. The difference between the maximum and minimum stresses is called stress range, $\Delta\sigma = \sigma_{max} - \sigma_{min}$. The average of the maximum and minimum stresses is called the mean stress, $\sigma_m = (\sigma_{max} + \sigma_{min}) /2$, and half the range is called the stress amplitude, $\Delta\sigma/2 = \sigma_a = (\sigma_{max} - \sigma_{min}) /2$. An important ratio to consider is the ratio of the maximum stress over the minimum stress, called the stress ratio, $R = \sigma_{max} / \sigma_{min}$. In our case the stress ratio R was equal to 0.1, meaning that the maximum stress was 10 times bigger than the minimum stress. Figure 11 shows a similar variation for the tension-tension applied stress during our fatigue testing.

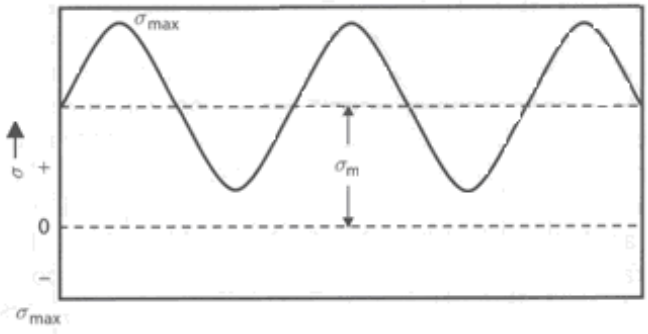

Figure 11. Tension-Tension with Applied Stress

At high stress levels the composite material will exhibit shear yielding, forming a yield zone at the crack tip, like metals. This is the result of increasing number of broken bonds during each cyclic load. Composite materials will show warnings before the part completely fractures. Figure 12 shows matrix cracking, fiber bridging, fiber

rupture, fiber pullout and fiber matrix debonding, most of the different signs of failure that can be found prior to fracture. Out-of-plane tensile stresses will cause most of the delamination or failure between plies due to the reduction in their ability to carry major loads. For the M55J/RS3, the 90° ply corresponds to the out-of-plane ply due to its stacking sequence.

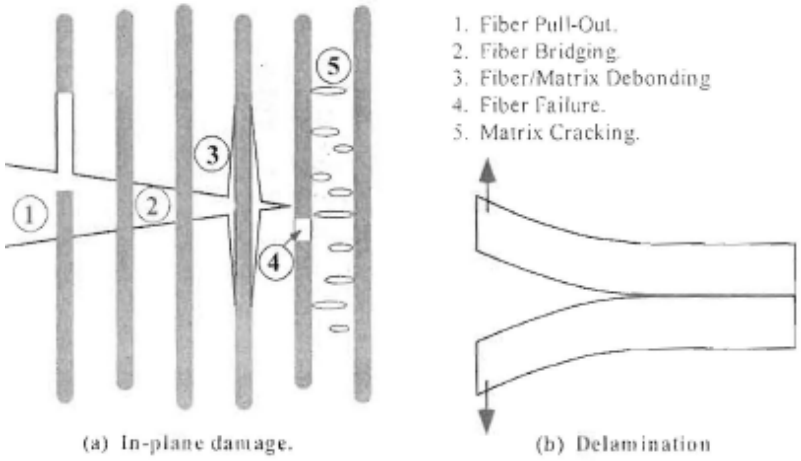

Figure 12. Damages in Fiber-Reinforced Composites

2.6 M55J/RS3 Failure Mechanisms

The type of failure mechanism depends essentially on the layup of the material, and the type of loading. For laminates that have off-axis plies like the M55J/RS3 with stacking sequence $[0, 90, +\text{-}45]_S$, most of the time the first and most profuse damage mode is matrix cracking. During cyclic loading, cracks form through the thickness of the plies, aligned parallel to the fiber direction and perpendicular to the to the 0° ply, which in this case is the dominant load axis. It can be said then that initial damage will occur in the 90° ply, the weakest ply in the stacking sequence. This resulting damage in the

material's structure will cause a reduction in strength, and will also affect the expected service life of the part.

As the cyclic load is repeated, existing cracks will extend and new cracks will form. Delamination will develop between the damaged 90° ply and the 45° ply causing the 45° plies to eventually fail. In the mean time transverse stresses will cause the 0° to experience matrix cracking. Lastly, the fatigue multiplication effect will cause the 0° plies to fail causing total failure.

The separation of the individual plies is called delamination and is the result of high stress concentration near the free edges and in discontinuities. Out-of Plane loads are mostly responsible for the delamination of a bonded composite. During testing it is fairly common to observe such behavior in most of the specimens. Delamination is constrained to grow between individual plies, along the entire length of the specimen, and is not supposed to be directly responsible for the total failure of the material. Other signs of failure such as fiber break or pull-out and fiber/matrix debonding will only occur when the matrix has a higher ultimate strain than the carbon fiber. In Chapter 4 we will discuss the failure mechanisms found after testing the 4 different M55J/RS3 composite configurations at different stress levels.

2.7 Summary

The natural space environment represents a test to spacecraft structures and electronic components. The most dangerous threats are radiation and ESD which can lead to degradation and eventually catastrophic failure of spacecraft structure and electronics. It is vital that any improvements made in materials used for space applications provide the required EMI shielding protection and conduction to avoid ESD

problems. The purpose of this study is to investigate the changes in the electrical properties of the 4 configurations of the M55J/RS3 material while being subjected to different cyclic stress levels. Results of the study will show if the resistance and EMI measurements of a M55J/RS-3 composite with nickel nanostrands™ is affected due to the application of different UTS levels of cyclic loads.

III. Method of Experimentation

3.1 Introduction

This chapter discusses how all the specimens were prepared and tested. We will also go over the testing sequence and the equipment used to accomplish the different tasks. The objective of this chapter is to familiarize the reader and prospective students with the testing procedures involved in this experiment that will aid in the expansion of the research effort.

3.2 Specimens Preparation

For this study we evaluated 4 different configurations of the M55J/RS3 material, three of which had Nickel nanostrands added in different locations of the laminate. The composite material was initially placed between 2 thin plastic sheets for protection. All specimens were cut from a panel, by the AFIT machine shop, using a high pressure water jet cutter to a final dimension of 15.25 x 2.7cm each. The average thickness of the specimens was 0.1016 cm. Figure 13 illustrates the testing specimen.

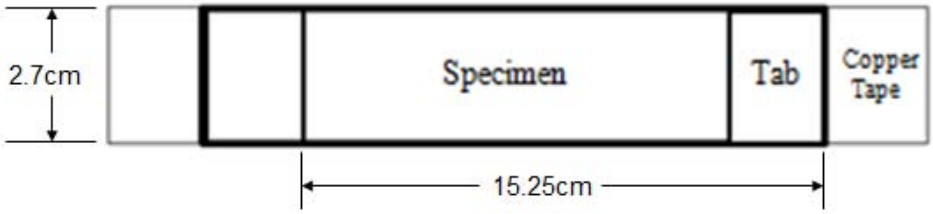

Figure 13. M55J/RS-3 Testing Specimen

3.3 Fatigue Testing Equipment and Procedures

For the fatigue testing it was necessary to bond glass/epoxy tabs on the gripping section in order to avoid crushing the specimen. The tabs had an average size of 2.54 x 2.7cm and were bonded using the M-Bond 200 adhesive. Copper tape was added to the

ends of the specimens by the manufacturer with the purpose of measuring the resistance across the sample before and after each cyclic load was applied to the material.

The fatigue testing was performed using the Material Testing Station (MTS) 810, a servo hydraulic testing system with a capacity of 22 Kips (98kN). This machine employs transistor technology and close loop automation concepts to develop a high-rate test system that use a double-action hydraulic piston, controlling the desired force or strain imposed on a specimen. Fatigue testing was performed in the AFIT laboratory, bldg. 640, room 254, and all specimens were tested at room temperature. Four stress levels were selected for this task. Stress levels were 60%, 70%, 75% and 90% of the UTS for each specimen configuration. The 70% UTS stress level was used as a preliminary data gathering test. The 60%, 75% and 90% were used to analyze the material's behavior after the cyclic was applied. For the 90% UTS we concentrated our efforts in EMI testing due to separation of copper tape from material during specimens' cutting phase, for the midplane and interlaminar specimens.

The first step in the process before running a procedure in the MTS 810 system was to open the Station Manager program and create a configuration file with the Station Builder program. After the configuration file was created, hydraulic pressure was applied to the station. The MTS machine was warmed up for about 30 minutes, in accordance with manufacturer's guidelines. For each test a grip pressure of 8.2 MPa (1.2Ksi) was applied by the MTS647 hydraulic wedge grips. After warm-up the grips were moved to properly accommodate the specimen. The specimen was placed in a way such that each grip covered an equal amount of material.

Before starting each test, a level was used to properly align the specimen in the vertical direction, with the purpose of avoiding the development of unwanted shear stresses into the material. After the specimen was properly placed and aligned, an extensometer was mounted on the specimen to record strain. An R ratio of 10 and a frequency of 10Hz were maintained for all stress levels. The required sets of cyclic loads, parameters and specifications were controlled by the Station Manager program. Figure 14 shows the MTS 810 system used for the fatigue testing.

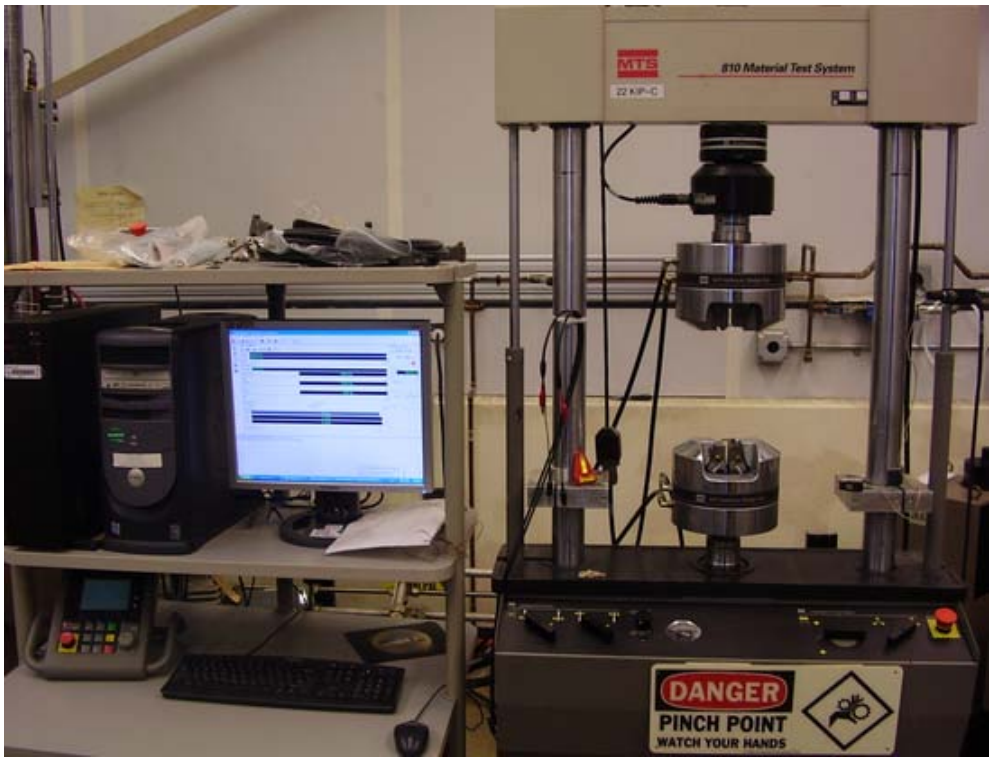

Figure 14. MTS 810 System

Using the Station Builder program we set Station Limits, and readout devices to monitor station signals. Lastly, using the Multipurpose Testware program we created the procedure, specifying the parameters, sequence of events, and data gathering

requirements (i.e. *Force, Force Command, Displacement, Displacement Control, and Strain).* Figure 15 shows the applications of the station manager program.

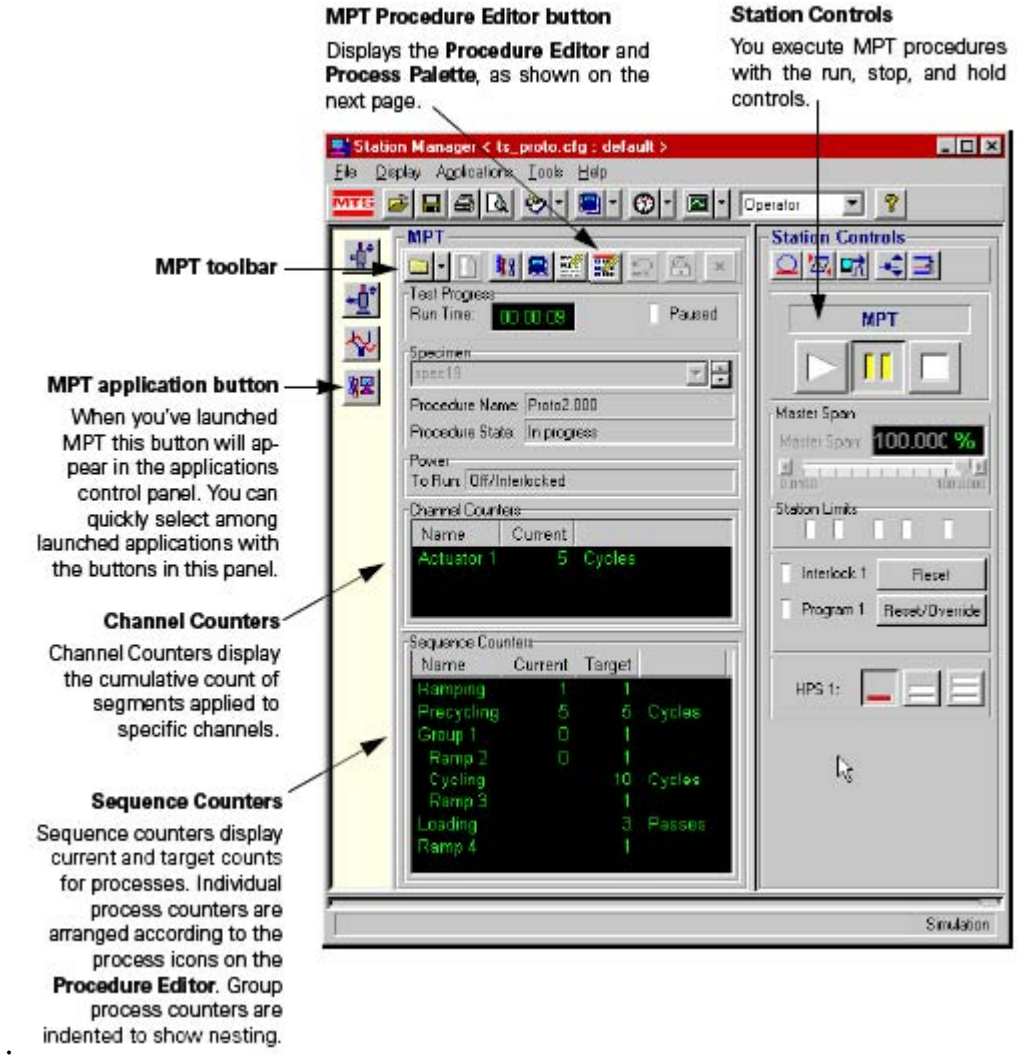

Figure 15. Station Manager Program

One of the most important parameters to identify is the range of the "Detectors". This function allows the user to specify how much load (maximum and minimum) and how much strain (maximum and minimum) it will be allowed during the test. If those limits are reached anytime, the machine will shutdown to protect the specimen. After

setting all procedures and parameters in the Station Manager program, everything was ready to start mounting our specimens into the test fixture.

To start testing we proceeded to grip the top part first on displacement mode. Next step was to go from displacement mode to force mode, followed by signal Offset, and finally gripping the lower part. Last step was to verify the procedure, parameters, and setting so we could lock the procedure and finally press the “Run or Play” command to start the test. At the end of the test we proceeded to unlock the procedure, ungrip bottom part first in force mode. Last step was to change from force mode to displacement mode to ungrip bottom part. A complete test sequence can be found in Appendix A.

3.4 MPT Procedure Editor

The MPT Procedure Editor is the application where the input for the fatigue test sequence is specified. Parameters such as stress levels, number of cycles, acquisition sampling, and other parameters are specified for each configuration and stress level. Each configuration will have a different input due to the difference in their mechanical properties. Figure 16 shows the fatigue testing sequence followed in this effort.

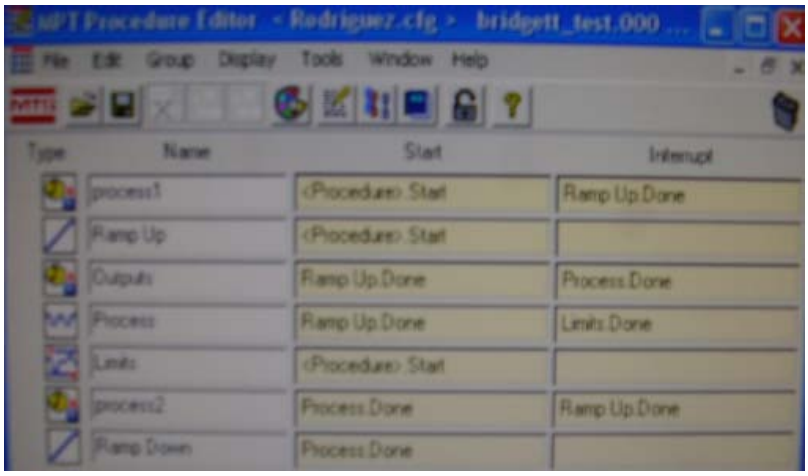

Figure 16. MPT Procedure Editor Test Sequence

3.5 EMI Test Equipment and Procedures

EMI tests were performed before and after each fatigue using the Agilent Technologies E8362B PNA Series Network Analyzer and Calibration Kit X11644A. The PNA analyzer has a pair of ports to which the test device is connected by means of flexible cables. For this task the specimen was placed between the ends of the flexible cables, where the sample holder kept the material in place. EMI tests had the objective to measure transmittance (in dB) of the material and to document the change after a cyclic load was applied to the specimen. This task was performed at the AFRL Material's Laboratory facilities at room temperature. The EMI test procedure consisted of three parts: settings, calibration, and measurements.

3.5.1 Settings Procedure

The settings part consisted in the verification and correction of the testing parameters. Below is shown the procedure for this part.

- ***Start Up***
- ***Program Network Analyzer***
- ***Sweep***
    - ***Data points (select 201 points)***
    - ***Sweep type (select linear)***
- ***Press Start : 8.2 GHz***
- ***Press Stop: 12.4 GHz***
- ***Channel (5.00 dBm)***

3.5.2 Calibration

Calibration was the second part of this test sequence and was needed prior making any measurements, to ensure we were getting accurate EMI measurements. When properly calibrated for each frequency in the data set, the analyzer will determine if there

are any undesired parameters that may be removed or suppressed from the test sample data. Below is shown the calibration procedure for this part.

- ***Go to Calibration Wizard***
  - ***Select unguided***
  - ***Check create new cal set***
  - ***Select TRL 1-2 port (for Thru & Line)***
  - ***View of Select Cal Kit: X BAND (scroll down to #28 - Calibration Kit X11644A)***
- ***To start calibrating:***
  - ***Take out plastic caps.***
  - ***Insert short wave plate (solid plate) between cables and secure it using long screws on 4 corners.***
  - ***Run SHORT port 1 and run SHORT port 2.***
  - ***Remove short wave plate.***
  - ***Insert Line wave plate (plate with square hole) between cables and secure it using long screws on 4 corners.***
  - ***Run Line and select ¼ wavelength line.***
  - ***Remove line wave plate.***
  - ***Without placing a plate between the cables run THRU.***
  - ***Click next & Finish.***
- ***Go to window***
  - ***Measurement set up: select Set up B***
- ***Insert Sample***
  - ***Go to channel – Average – 16 scans and click Average On Ok***
  - ***Right Click Auto Scale on each window (red outline appears)***
  - ***Arrow shows transmittance average values.***

  - ***Left Click***
    - ***File--Save As--Save in (write name of file)--Save as Type: Trace *.prm (for each window)***

After the machine was calibrated we proceeded to take measurements. In order to ensure that we kept a consistent and accurate reading process, a red or black mark was placed on the specimen. This mark was used to ensure next time we were making a reading we evaluated the exact same spot we were evaluating previously. Figure 17 shows a picture of a marked specimen, and Figure 18 shows the test set-up for this part.

Figure 17. Red Mark on Specimen

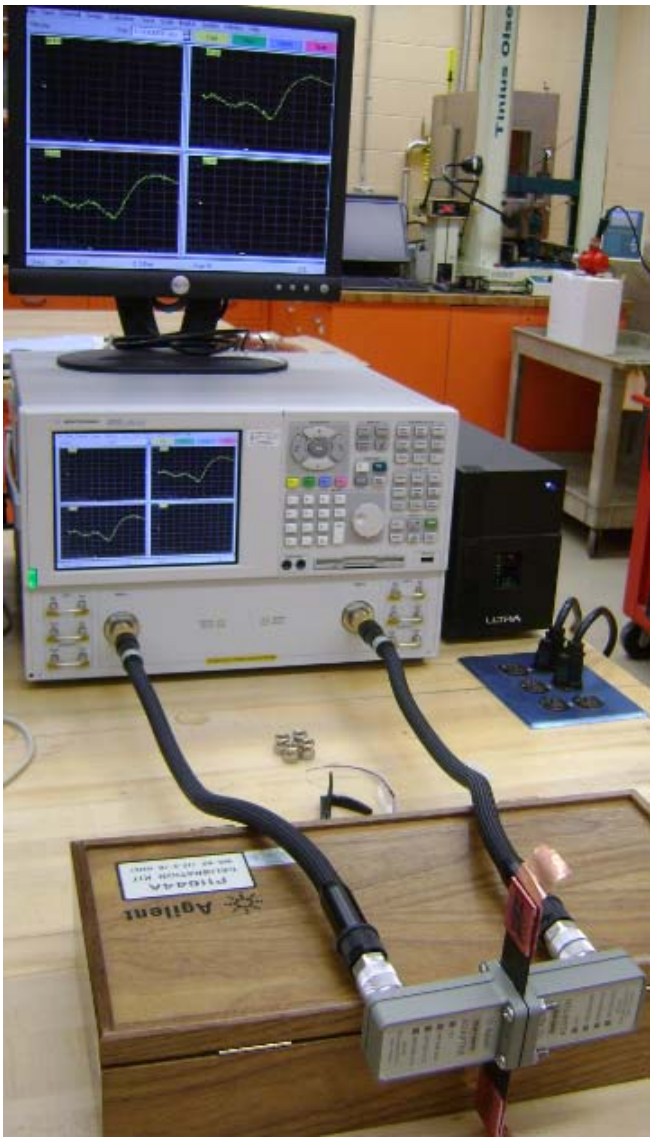

Figure 18. EMI Test Set-Up

3.6 Resistance Testing

Resistance testing was performed also at the AFRL Material's Laboratory facilities, where the Extech 380560 Milliohm meter was provided to take the resistance measurements. Figure 19 shows the Extech Milliohm Meter used for this study. The purpose of this task was to measure the resistance across the sample before and after each cyclic load was applied to the material, and to document the change. Below is shown the resistance testing procedure followed during the test.

- ***Connect cables (have the white cable on top on both sides).***
  - ***White cable goes in the sense inlet.***
  - ***Black cable goes in the force inlet.***
- ***Turn power on.***
- ***Set the scale to 2 ohms.***
- ***Write down measurements.***
- ***Turn power off & Disconnect***

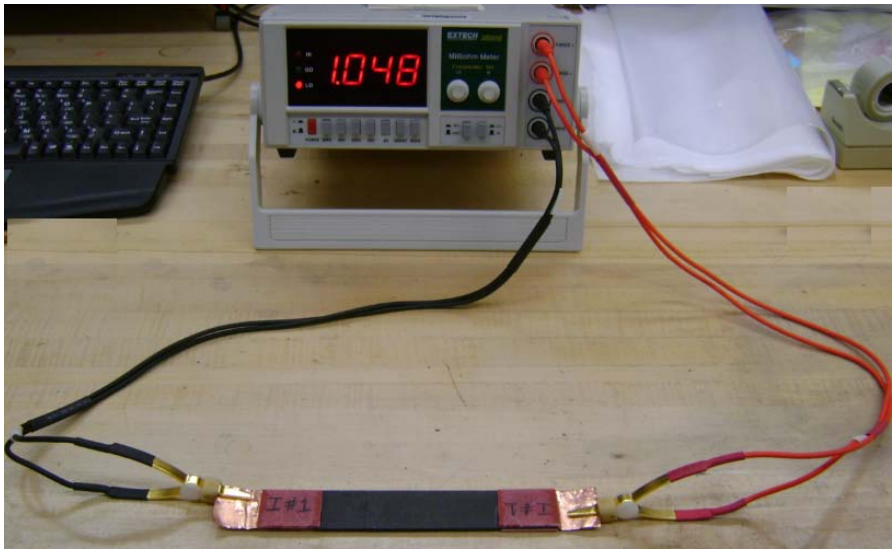

Figure 19. Extech Milliohm Meter

3.6 Test Plan Summary

The tasks performed during this research effort were performed as described herein. Fatigue testing was conducted on 15.25 x 2.7 cm coupons with copper tape laminated at both ends of the composite in order to measure the resistance across samples. Specimens of 4 different configurations were tested: Control (had no Ni nanostrands), Exterior, Midplane, and Interlaminar configurations, which had Ni nanostrands added in different locations of their laminate. Glass/epoxy tabs were necessary to protect the specimen against possible damage caused by the MTS grips. The 2.54 x 2.7 cm (1 x 1.0625 in) tabs were attached to the specimens using M-Bond 200 adhesive. Fatigue testing began once the specimen was properly mounted in the MTS 810 servo-hydraulic testing machine, applying a grip pressure of 8.2 MPa (1.2 ksi) in all tests. The frequency used during the test was 10 Hz. Selected stress levels were 60%, 70%, 75% and 90% of the UTS with an R ratio of 10. Resistance & EMI tests were performed before and after each fatigue test, in order to document and evaluate changes in the electrical properties. Table 1 shows the UTS values for the four configurations and Table 2 shows all the tested specimens and what was tested on each configuration.

Table 1. Specimens' UTS Values

Configuration	UTS
Control	408 MPa (59 ksi)
Exterior	475 MPa (69 ksi)
Midplane	500 MPa (72.5 ksi)
Interlaminar	414 MPa (60 ksi)

Table 2. Tested Specimens

Configuration - Stress Level	Stress Range	EMI	Resistance	Fatigue
Control - 60% UTS	24.28 MPa to 244.8 MPa (3.54 ksi to 35.4 ksi)	X	X	X
Exterior - 60% UTS	28.5 MPa to 285 MPa (4.14 ksi to 41.4 ksi)	X	X	X
Midplane - 60% UTS	30 MPa to 300 MPa (4.35 ksi to 43.5 ksi)	X	X	X
Interlaminar - 60% UTS	24.84 MPa to 248.4 MPa (3.6 ksi to 36 ksi)	X	X	X
Control - 70% UTS	28.56 MPa to 285.6 MPa (4.13 ksi to 41.3 ksi)	-	X	X
Exterior - 70% UTS	28.5 MPa to 285 MPa (4.83 ksi to 48.3 ksi)	-	X	X
Midplane - 70% UTS	35 MPa to 350 MPa (5.075 ksi to 50.75 ksi)	-	X	X
Interlaminar - 70% UTS	28.98 MPa to 289.8 MPa (4.2 ksi to 42 ksi)	-	X	X
Control - 75% UTS	30.6 MPa to 306 MPa (4.425 ksi to 44.25 ksi)	X	X	X
Exterior - 75% UTS	35.63 MPa to 356.3 MPa (5.175 ksi to 51.75 ksi)	X	X	X
Midplane - 75% UTS	37.5 MPa to 375 MPa (5.438 ksi to 54.38 ksi)	X	X	X
Interlaminar - 75% UTS	31.05 MPa to 310.5 MPa (4.5 ksi to 45 ksi)	X	X	X
Control - 90% UTS	36.72 MPa to 367.2 MPa (5.31 ksi to 53.1 ksi)	X	X	X
Exterior - 90% UTS	42.75 MPa to 427.5 MPa (6.21 ksi to 62.1 ksi)	X	X	X
Midplane - 90% UTS	45 MPa to 450 MPa (6.525 ksi to 65.25 ksi)	X	-	X
Interlaminar - 90% UTS	37.26 MPa to 372.6 MPa (5.4 ksi to 54 ksi)	X	-	X

IV. Analysis and Results

4.1 Introduction

The purpose of this chapter is to report the results obtained for the 4 different configurations of the M55J/RS3 material, three of which had nickel nanostrands™ added in different locations in the laminate (i.e. exterior, midplane, interlaminar). All 4 configurations consisted of a symmetric 8 plies layup of M55J/RS3 composite material with its fibers oriented at 0/90/45/-45 degrees. Figure 20 shows the 4 configurations of the M55J/RS-3 composite material.

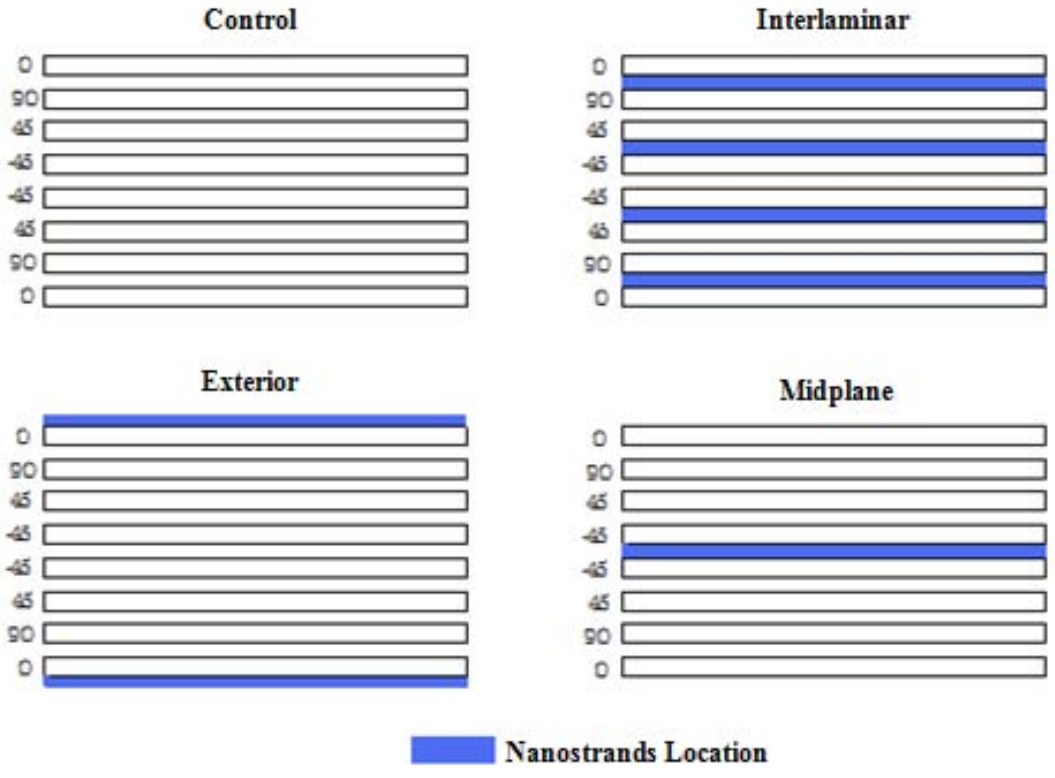

Figure 20. M55J/RS-3 Composite Configurations

4.2 Resistance Measurements

The Extech Milliohm Meter was used to register the material's resistance value before and after each set of cyclic load was applied. Fatigue Stress levels applied were 60%, 70%, 75% and 90% for each specimen configuration. For the 90% UTS level it was not possible to get accurate resistance measurements for the midplane and interlaminar configurations due to copper tape damage during processing/cutting operation. Results for the 70% UTS level were only used to get a preliminary tendency for each configuration behavior.

4.2.1 Resistance for 70% UTS Level

The specimens used for this level are denominated "old specimens" because they were manufactured from an older panel, different from the panel used for the 60%, 75%, and 90%UTS level specimens. Some of these "old specimens" had monotonic tension load previously applied to them. Also these "old specimens" had a copper mesh at the ends instead of copper tape as used in the 60%, 75%, and 90%UTS level specimens. As previously mentioned, the 70% UTS level was used only to know how each configuration would respond after the application of cyclic loads. Table 3 contains the recorded values for the 70% UTS level.

Table 3. Resistance for 70% UTS Stress Level

Cycles Applied	Control 28.56 MPa to 285.6 MPa (4.13 ksi to 41.3 ksi)	Exterior 28.5 MPa to 285 MPa (4.83 ksi to 48.3 ksi)	Interlaminar 28.98 MPa to 289.8 MPa (4.2 ksi to 42 ksi)	Midplane 35 MPa to 350 MPa (5.075 ksi to 50.75 ksi)
0	0.499 Ω	0.127 Ω	0.153 Ω	0.304 Ω
10,000	1.374 Ω	0.128 Ω	0.225 Ω	0.46 Ω
20,000	1.534 Ω	0.128 Ω	0.233 Ω	0.489 Ω
30,000	1.578 Ω	0.128 Ω	0.234 Ω	0.499 Ω
40,000	1.654 Ω	0.128 Ω	0.235 Ω	0.507 Ω

From the recorded data in Table 3 we can see that the control specimen kept increasing its resistance values. This configuration had some load previously applied that seemed to rapidly increase the specimen's resistance during the first 10,000 cycles. Also, the control specimen doesn't have nickel nanostrands™, it only has the graphite fibers serving as it conductive medium. The application of cyclic loads damages the graphite fibers, making disruptions in the flow of current and ultimately creating an increase in the resistance across the material. We can see that after applying the first 10,000 cycles the resistance increased more than 300%. The exterior configuration had graphite fibers and nickel nanostrands serving as conductive mediums. The application of cyclic loads caused to the damage on the graphite fibers, but the increase in the resistance across the material was almost negligible. Contrary to the control configuration we didn't see a significant increase in the resistance measurements. After applying the cyclic loads it was registered less than 1% increase in the exterior configuration's resistance. The conduction for this configuration seemed to be constant as long as the integrity of the nickel nanostrands™ and the integrity of the material were preserved.

The recorded data also shows the midplane and interlaminar specimens kept increasing their resistance values with the application of fatigue loads. Both configurations contained nickel nanostrands that improved their conduction. It was observed that for both configurations the biggest increase in resistance was after applying the first 10,000 cycles. The resistance measurements for the interlaminar configuration increased 53% while the midplane increased 67%. Up to this point, the increase for the midplane configuration was a little higher than the increase for the interlaminar. A possible reason for this could be the capacity of the interlaminar configuration to conduct

electric charge without having to go too deep into the material as in the case of the midplane configuration. Comparing all 4 specimens we see the exterior configuration performing better than the rest of the specimens. This had to do mainly with the capacity of nickel nanostrands™ to conduct the electric charge along the surface of the material without having to go into the material as the other configurations. After this preliminary test, the exterior configuration performed better, followed by the interlaminar, midplane, and control configurations. The purpose of this preliminary test was to get familiar with the procedure and to see a trend on the behavior of each configuration. After applying 40,000 cycles we were able to see the trend and Figure 21 shows the results for the 4 specimens' configurations.

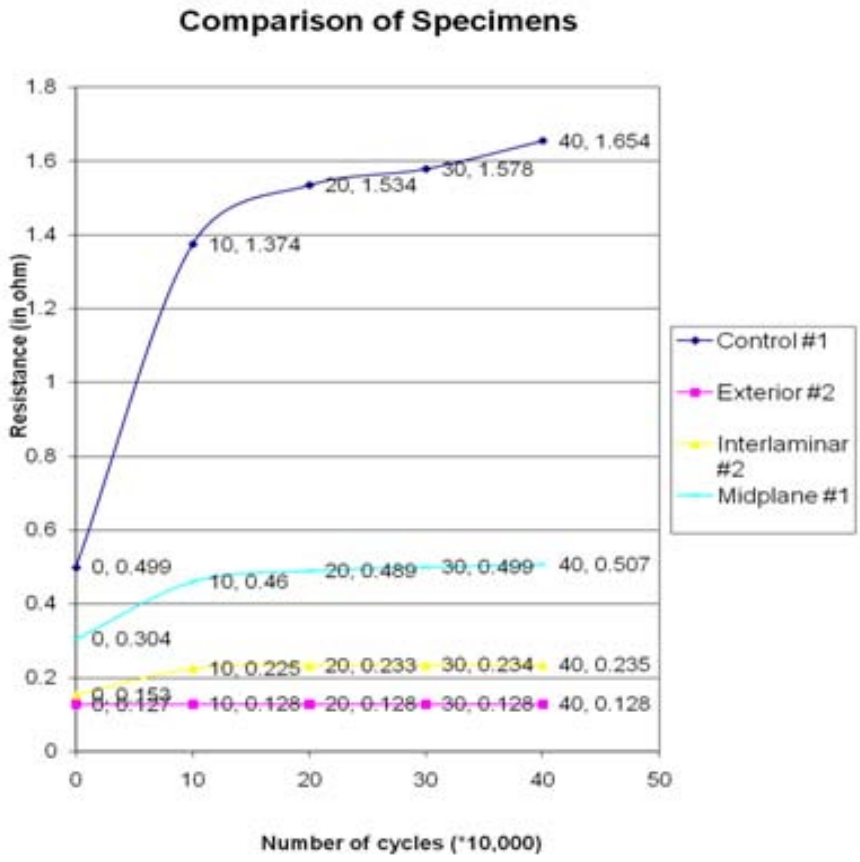

Figure 21. Resistance Comparison for 70% UTS Level

4.2.2 Resistance for 60% UTS Level

The 60% UTS served as our first stress level to compare the trends obtained from the 70% UTS level. At this stress level 2 million cycles were applied to the control, exterior, and midplane configurations. Only 1.5 million cycles were successfully applied to the interlaminar configuration. An unexpected increase in the grip pressure caused damage to the specimen before applying the last 500,000 cycles. From the recorded data shown in Table 3 we can see that the control specimen kept increasing its resistance values. After 2 million cycles its resistance increased 40%. The conduction for the control configuration seemed to be relatively constant for the first 3,000 cycles, but as in our previous 70%UTS case we see an increase after applying the first 10,000 cycles. The conduction for the exterior configuration seemed to be relatively constant for the first 22,000 cycles. After applying the 2 million cycles its resistance increased just 12%, mainly due to the nickel nanostrands™ that kept the conduction of the material. Table 4 shows the data for the 60% UTS level.

Table 4. Resistance for 60% UTS Level

	Control	Exterior		Interlaminar	Midplane
	24.28 MPa to 244.8 MPa	28.5 MPa to 285 MPa		24.84 MPa to 248.4 MPa	30 MPa to 300 MPa
	(3.54 ksi to 35.4 ksi)	(4.14 ksi to 41.4 ksi)		(3.6 ksi to 36 ksi)	(4.35 ksi to 43.5 ksi)
Total # of Cycles	Resistance (Ohm)	Resistance (Ohm)	Total # of Cycles	Resistance (Ohm)	Resistance (Ohm)
0	0.128	0.125	0	0.162	0.153
500	0.13	0.125	25,000	0.166	0.159
2,500	0.13	0.125	50,000	0.167	0.16
12,500	0.133	0.126	100,000	0.169	0.162
22,500	0.135	0.126	500,000	0.17	0.163
32,500	0.136	0.127	1,000,000	0.172	0.164
42,500	0.139	0.127	1,500,000	0.172	0.167
142,500	0.149	0.129	2,000,000	-	0.168
242,500	0.165	0.131			
500,000	0.172	0.133			
1,000,000	0.174	0.135			
1,500,000	0.177	0.138			
2,000,000	0.179	0.14			

The data for the interlaminar and midplane configurations show that they also kept increasing their resistance values with an increase in the number of applied cycles. The interlaminar specimen data shows that after applying 1.5 million cycles its resistance increased 6%. For the midplane specimen, after applying 2 million cycles its resistance increased 10% from its initial value. To have a fair comparison among all the specimens we also compared the results for 1.5 million cycles. Up to this point the control specimen increased 38%, the exterior configuration increased 10%, the interlaminar increased 6%, and the midplane configuration increased 9%. It catches our attention that even after 2 million cycles were applied, the initial resistance value for the interlaminar and midplane configurations were higher than the final value of the exterior specimen. The results of this test seemed to agree with the trend of our preliminary 70%UTS test, where the exterior configuration performed better followed by the interlaminar, midplane, and control configurations. The degree of performance exhibited by all configurations had to do mainly with their capacity to conduct the electric charge near the outer surface instead of going through the material. Figure 22 shows the performance of the 4 specimens during the test.

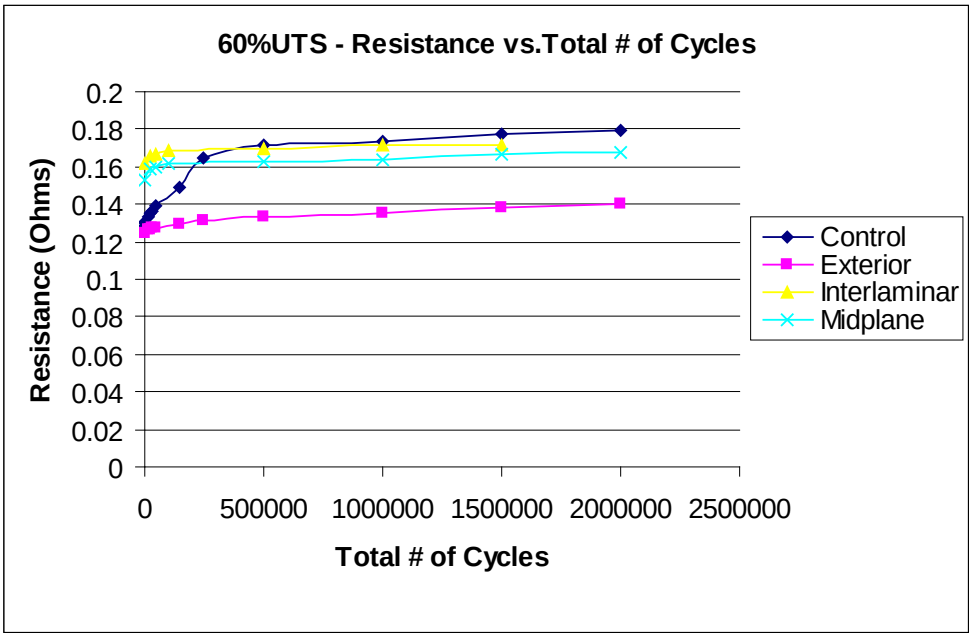

(a)

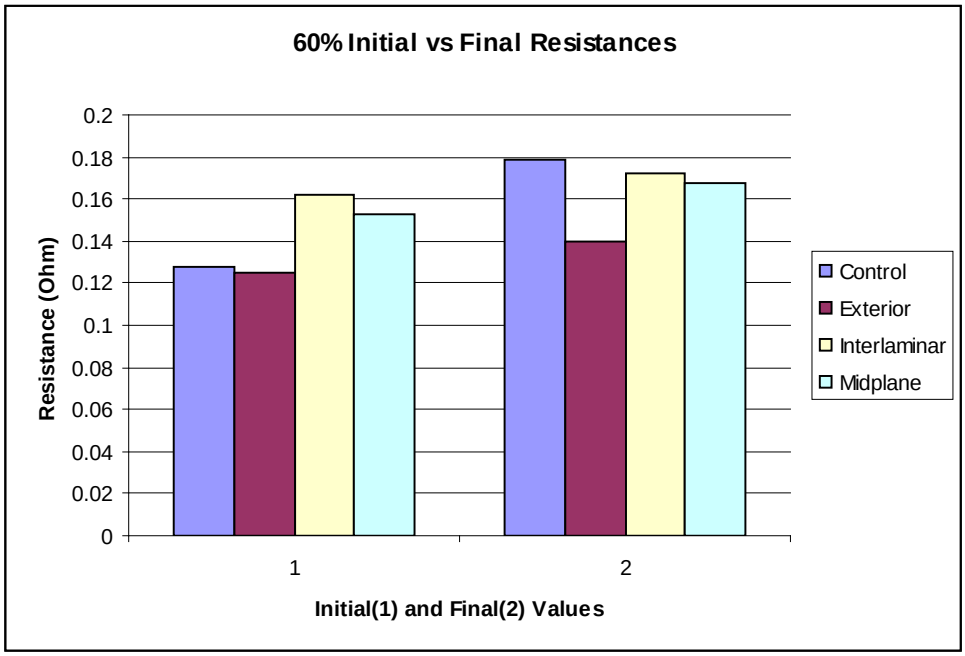

(b)

Figure 22. (a)Resistance Comparison (b) Initial vs. Final Values for 60% UTS Level

Initial and final resistance values for 60% UTS level were also normalized to observe how the resistance changes in all configurations contrasted to the initial value of the control specimen. Figure 23 shows the normalized resistance values for 60% UTS stress level. The plotted data shows that at the end of the test all configurations containing nickel nanostrands™ performed better than the control specimen.

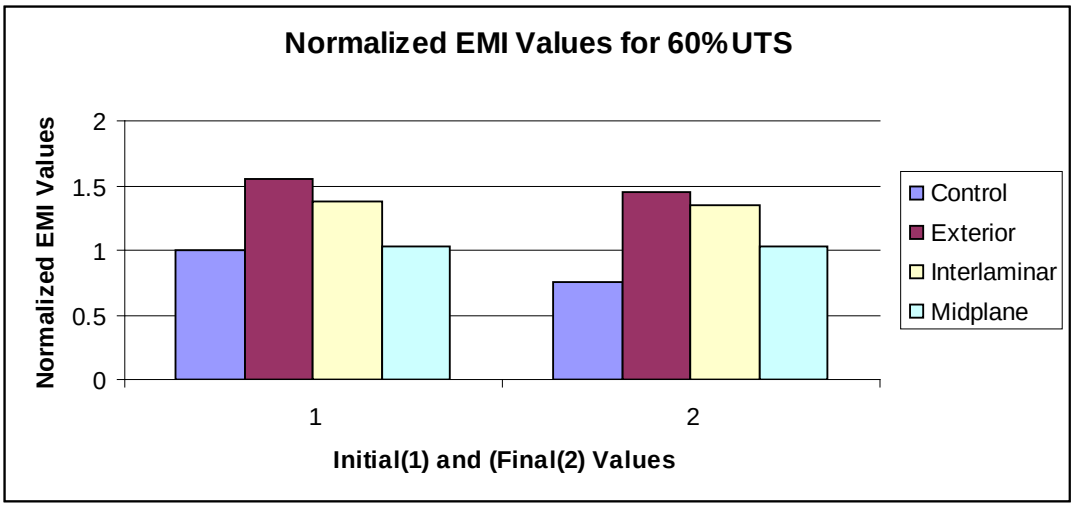

Figure 23. Normalized Resistance Values for 60% UTS Level.

4.2.3 Resistance for 75% UTS Level

The number of cycles applied to the control, exterior, and midplane configurations varied according to their capacity to withstand the load. From the recorded data we can see that the control specimen kept increasing its resistance values until it finally failed after 366,000 cycles. After the application of the cyclic load its resistance increased 100%, doubling its original value. It is clear how an increase in stress affects and increases the resistance of the control specimen. On the other hand, the exterior configuration seemed to have very little increase on its resistance up to the failure point. After 43,000 cycles its resistance increased a 7% from its initial value. The electrical

properties for the exterior configuration kept showing a constant trend, but its mechanical failure after such a low amount of cycles when compared against the control specimen causes concern. Table 5 shows the data for the 75% UTS level.

Table 5. Resistance for 75% UTS Level

	Control	Exterior		Interlaminar	Midplane
	30.6 MPa to 306 MPa	5.63 MPa to 356.3 MPa		31.05 MPa to 310.5 MPa	37.5 MPa to 375 MPa
	(4.425 ksi to 44.25 ksi)	(5.175 ksi to 51.75 ksi)		(4.5 ksi to 45 ksi)	(5.438 ksi to 54.38 ksi)
Total # of Cycles	Resistance (Ohm)	Resistance (Ohm)	Total # of Cycles	Resistance (Ohm)	Resistance (Ohm)
0	0.125	0.122	0	0.528	0.276
2,000	0.128	0.122	2,000	0.663	0.325
10,000	0.136	0.126	10,000	0.712	0.328
25,000	0.143	0.131	25,000	0.748	0.332
50,000	0.155	Failed @ 43,000	50,000	0.757	0.333
75,000	0.161		100,000	0.788	Failed @ 50,300
100,000	0.177		200,000	0.802	
150,000	0.18		300,000	0.876	
175,000	0.185		350,000	0.879	
225,000	0.188		500,000	1.014	
300,000	0.196		750,000	1.017	
363,500	0.252		1,000,000	1.048	
	Failed @ 366,000				

The 75%UTS data for the exterior specimen shows a value of 0.131ohm after 25,000 cycles were applied. The same resistance value was registered for the 60% UTS data after 242,500 cycles were applied. At the lower 60% level it took ten times the same amount of cycles (250,000) to increase the resistance to the same amount registered at the 25,000 cycles point at 75%UTS. It is clear that a significant increase in the stress level will greatly impact the electrical properties of the material. At the same time, the increase in stress level reduced the ability of the exterior specimen to withstand load. The exterior specimen was only able to withstand less than 3% of the amount of cycles applied at 60%UTS. When we take a look at the control's specimen final value for the 60%UTS after 2 million cycles (0.177ohm), it was the same amount registered at the

75%UTS just after 150,000 cycles. For a 15% increase in stress, it took 1,850,000 less cycles to increase the resistance to the same value. We can also see how the increase in stress affects the structural integrity of the specimens. At a 60%UTS and after 2 million cycles were applied to the control specimen it delaminated, but did not failed. At the 75% UTS level the specimen failed after experiencing less than 20% the amount of cycles experienced by the 60%UTS specimen.

The data for the interlaminar and midplane configurations showed that they also kept increasing their resistance values with an increase in stress level and with the application of cyclic loads. The midplane configuration failed after the application of 50,300 cycles, and its resistance increased 20% before fracture. This structural failure, similar to the case of the exterior configuration, causes concern after failing at less than 3% of the amount of cycles applied at 60%UTS. The data for the interlaminar specimen showed that after 1 million cycles were applied its resistance increased 98%, almost doubling its initial value, but without causing fracture of the specimen. This indicates that somehow the manner in which the nickel nanostrands^{TM} are distributed throughout the laminate it will not only affect the electrical properties, but also its mechanical properties, and crack propagation. For example the interlaminar configuration sustained the most number of cycles without experiencing total failure. A reason for this could be that the added nanostrands layer between the 0° and 90° plies acted as a barrier to crack propagation. The same could be said for the nanostrands layer between 45 and -45 plies.

The only common point for applied cycles where we have resistance values for all 4 configurations at this stress level is for 25,000 cycles. Up to this point results showed the control specimen increased 14%, the exterior configuration increased 6%, the

interlaminar increased 42%, and the midplane configuration increased 20%. When comparing the electrical properties of all four specimens we see the exterior configuration still performing better than the rest during this short period (first 25,000 cycles). We also need to mention that the interlaminar and midplane configurations could have done better as far as having lower initial resistance values and possibly lower percent increments. The higher initial values for these 2 configurations at the 75%UTS level had to do with the fact that the interface between the copper tape and the specimens were damaged during the specimens' preparation/cutting process. Figure 24 shows the performance of the 4 specimens during the test. Initial and final resistance values for 75% UTS stress level were also normalized to observe how the resistance changes in all configurations contrasted to the initial value of the control specimen. Figure 25 shows that at the end of the test the exterior configuration performed better than the rest of the specimens.

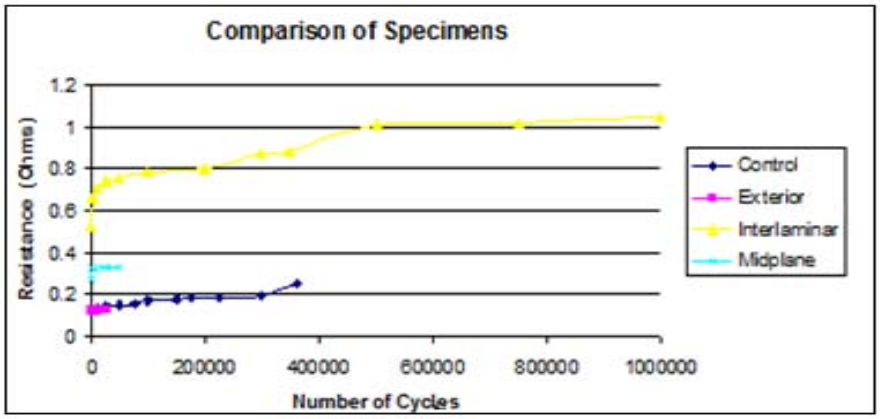

(a)

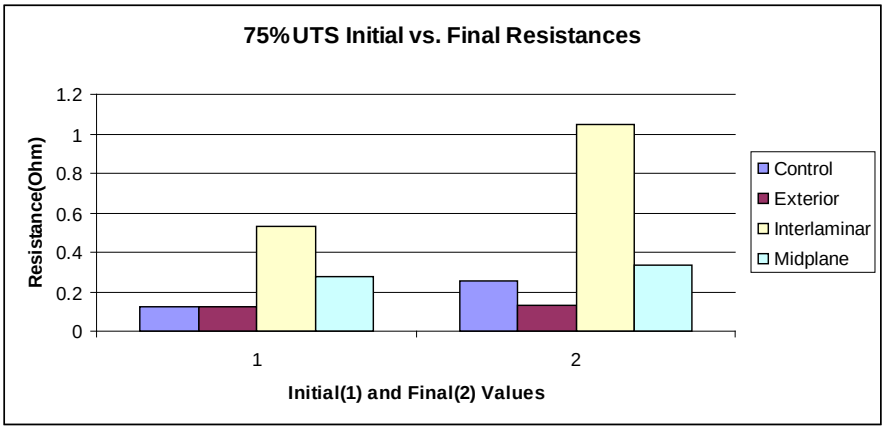

(b)

Figure 24. (a)Resistance Comparison (b) Initial vs. Final Values for 75% UTS Level

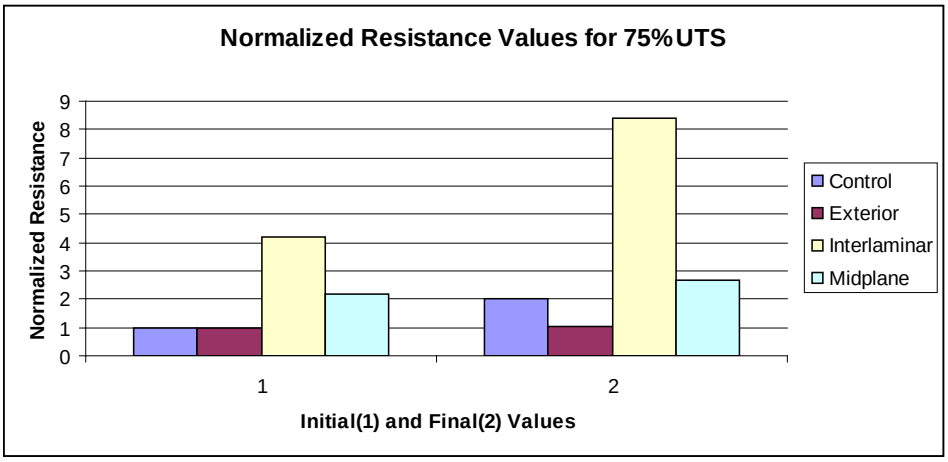

Figure 25. Normalized Resistance Values for 75% UTS Level.

4.2.4 Resistance for 90% UTS Level

The only configurations studied for resistance were the control and exterior configurations. The interlaminar and midplane configurations were not able to be accurately measured due to copper tape damage during the specimens' preparation/cutting process. The control specimen was able to withstand less than 8% of the amount of cycles experienced at 75%UTS and less than 2% of the amount of cycles

experienced at 60%UTS. The exterior specimen was able to withstand more amount of cycles than at 75%UTS, but only 11% of the amount of cycles experienced at 60%UTS. Table 6 shows the results for the control and exterior configurations for the 90% UTS level.

Table 6. Resistance for 90% UTS Level

	Control	Exterior
	36.72 MPa to 367.2 MPa	42.75 MPa to 427.5 MPa
	(5.31 ksi to 53.1 ksi)	(6.21 ksi to 62.1 ksi)
Total # of Cycles	Resistance (Ohm)	Resistance (Ohm)
0	0.124	0.125
10,000	0.132	0.126
25,000	0.146	0.128
50,000	Failed @ 27,470 cycles	0.129
100,000		0.131
225,000		0.135

When we compared the control's final 90%UTS resistance value vs. similar values at lower stress levels we see that a close value was obtained for the 60%UTS after 142,500 cycles were applied. It took 117,500 less cycles at a 30% higher stress level to increase the resistance value to the same point. When we compare the resistance values for the 25,000 cycles point for the 90%UTS and the 75%UTS, there is not too much difference between the obtained 0.143 ohm at 75%UTS and the 0.146 ohm obtained at 90%UTS. At the 60%UTS it might have took 200,000 cycles to increase the resistance value that took only 25,000 cycles at 90%UTS. The percent increment between 75% and 90% was much closer than the percent increment between 60% and 75% percent.

To our surprise the 90%UTS exterior specimen was able to survive more cycles at this level than at the previous 75%UTS level. Upon closer inspection we noticed that the panel from which the 90% exterior specimen was cut, measured 0.1816 cm instead of the

0.1016 cm that measured all other specimens, making the applied stress level (6.21 ksi to 62.1 ksi) considerably smaller than the intended 90% UTS level.

In general, the increase in resistance for the exterior specimen for the 60%, 75% and 90% was smaller than the increase in resistance for the control specimen. Figure 26 shows the performance of the 2 specimens during the test. Initial and final resistance values for 90% UTS stress level were also normalized to observe how the resistance changes in all configurations contrasted to the initial value of the control specimen. Figure 27 shows that at the end of the test the exterior configuration performed better than the control specimens.

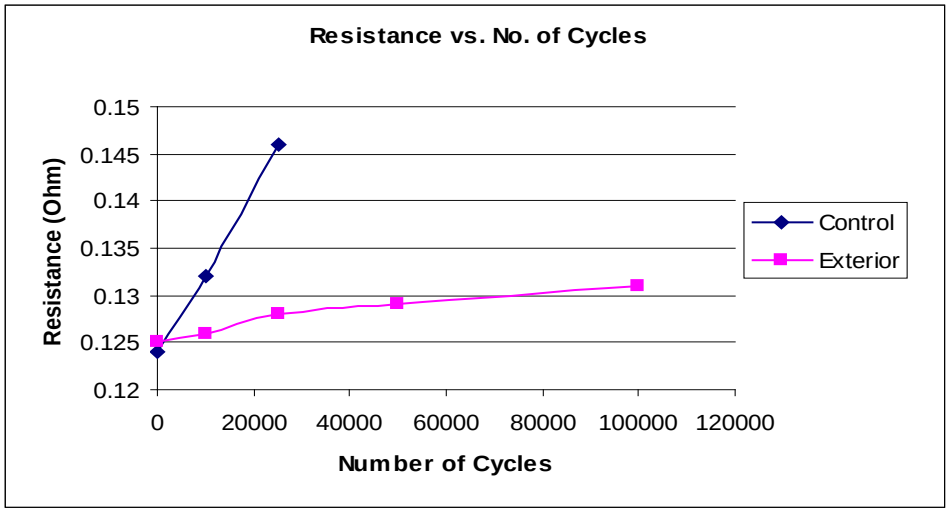

(a)

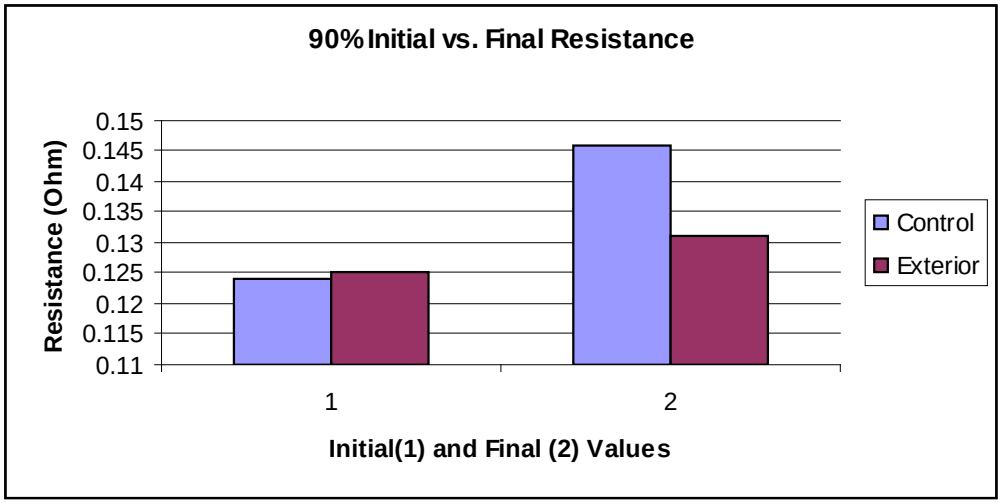

(b)

Figure 26. (a)Resistance vs. No. of Cycles (b) Initial vs. Final Values for 90% UTS Level

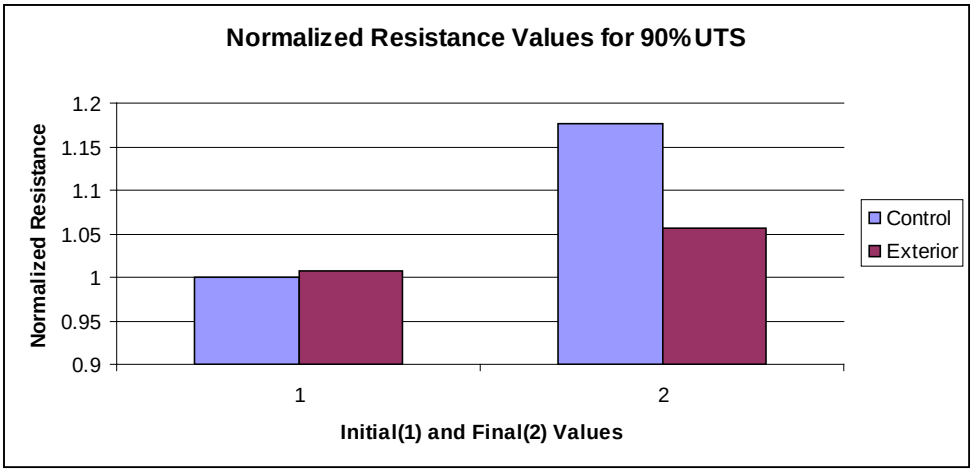

Figure 27. Normalized Resistance Values for 90% UTS Level.

4.3 EMI Shielding

The PNA Series Network Analyzer was used to register the specimens' EMI value before and after each set of cyclic load was applied. Fatigue stress levels applied were 60%, 75% and 90% of the UTS for each specimen configuration. Due to

unavailability of EMI equipment at the time, it was not possible to acquire the results for the preliminary 70% ultimate stress level.

4.3.1 EMI for 60% UTS Stress Level

The control specimen kept decreasing its EMI capability from the beginning. This configuration seemed to be highly affected with the addition of cyclic loads. After only applying 2% (42,500 cycles) of the total amount cycles (2 million) this configuration experienced 93% loss of its total loss during this test. After 2 million cycles the control specimen was able to retain just 75% of its initial EMI capability. Table 7 shows the data for the 4 configurations during the 75%UTS level test.

Table 7. EMI for 60% UTS Level

	Control	Exterior		Interlaminar	Midplane
	24.28 MPa to 244.8 MPa	28.5 MPa to 285 MPa		24.84 MPa to 248.4 MPa	30 MPa to 300 MPa
	(3.54 ksi to 35.4 ksi)	(4.14 ksi to 41.4 ksi)		(3.6 ksi to 36 ksi)	(4.35 ksi to 43.5 ksi)
Total # of Cycles	EMI (dB)	EMI (dB)	Total # of Cycles	EMI (dB)	EMI (dB)
0	58	90	0	80	60
500	52	90	25,000	80	60
2,500	52	90	50,000	80	60
12,500	48	90	100,000	80	60
22,500	47	90	500,000	80	60
32,500	46	90	1,000,000	78	60
42,500	45	90	1,500,000	78	60
142,500	44	90	2,000,000	-	60
242,500	44	90			
500,000	44	86			
1,000,000	44	86			
1,500,000	44	86			
2,000,000	44	84			

Of all 4 configurations, the exterior configuration had the highest initial EMI value of 90 dB. The nickel nanostrands™ provided an initial value that was 50% higher than the initial value of the control specimen. The exterior specimen kept its EMI value unchanged during the first 500,000 cycles, and then decreased 4% to 86dB for another million cycles. After 2 million cycles the specimen kept 93% of its initial EMI capability

for a final value of 84dB. This final value was 40% higher than the control's initial value, and 91% higher than the control's final value.

The interlaminar and midplane configurations kept their EMI values practically constant. The interlaminar initial EMI value of 80dB was 33% higher than the control specimen. This specimen saw a reduction of almost 3% percent. After 1.5 million cycles the specimen kept almost 98% of its initial EMI capability for a final value of 78dB. This final value was 30% higher than the control's initial value, and 77% higher than the control's final value. The midplane configuration kept its EMI values constant throughout the 2 million cycles, experiencing no reduction at all. The initial EMI value of 60dB was only 3% higher than the control specimen, but its final value was 36% higher than the control's final value. Just by looking at the data in Table 6, there's no doubt that the nickel nanostrands™ were effective in providing the required EMI protection. Figure 28 shows the EMI behavior for all specimens. It is clear that by adding nickel nanostrands™ the protection of the material was kept to an acceptable level, while the control specimen was not able to provide a sufficient EMI protection level. Figure 29 shows the normalized EMI values for the 60% UTS level.

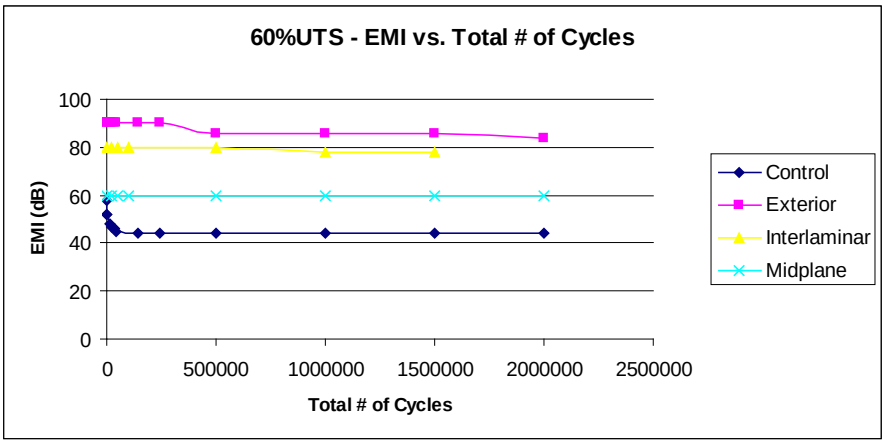

(a)

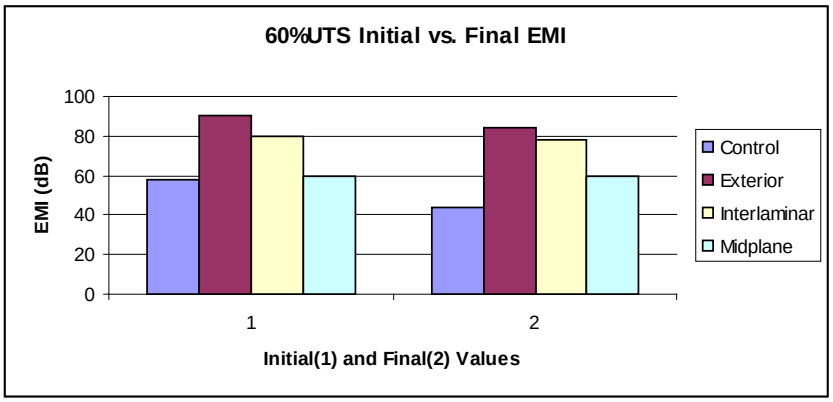

(b)

Figure 28. (a)EMI Comparison (b) Initial vs. Final Values for 60% UTS Level

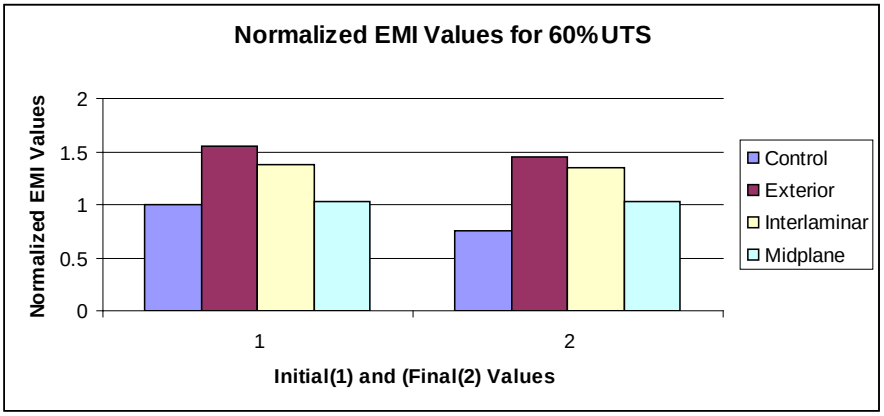

Figure 29. Normalized Resistance Values for 60% UTS Level.

4.3.2 EMI for 75% UTS Level

During this test the control specimen decreased its EMI capability after 300,000 cycles were applied. Surprisingly to us, its EMI value was constant through most of the test. After applying 363,500 cycles this configuration experienced 14% reduction, being able to retain just 86% of its initial EMI capability. The exterior specimen kept its EMI value unchanged up to fracture, which occurred after applying 43,000 cycles. The gathered data showed that the nickel nanostrands™ were effective in providing protection's. Its final 90 dB value was 80% higher than the control's final value. Table 8 shows the EMI data for the 75% UTS stress level.

Table 8. EMI for 75% UTS Level

	Control	Exterior		Interlaminar	Midplane
	30.6 MPa to 306 MPa	5.63 MPa to 356.3 MPa		31.05 MPa to 310.5 MPa	37.5 MPa to 375 MPa
	(4.425 ksi to 44.25 ksi)	(5.175 ksi to 51.75 ksi)		(4.5 ksi to 45 ksi)	(5.438 ksi to 54.38 ksi)
Total # of Cycles	EMI (dB)	EMI (dB)	Total # of Cycles	EMI (dB)	EMI (dB)
0	58	90	0	80	60
2,000	58	90	2,000	80	60
10,000	58	90	10,000	80	60
25,000	58	90	25,000	80	60
50,000	58	Failed @ 43,000	50,000	80	57
75,000	58		100,000	80	Failed @ 50,300
100,000	58		200,000	80	
150,000	58		300,000	78	
175,000	58		350,000	74	
225,000	58		500,000	70	
300,000	58		750,000	70	
363,500	50		1,000,000	68	
	Failed @ 366,000				

The midplane configuration kept its EMI values practically constant while it was structurally sound. As in the exterior configuration case, the nickel nanostrands™ were effective, and were not damaged until the specimen totally failed. This configuration experienced a reduction of 5% before failing, and its 57 dB value was 14% higher than the control's final value. The interlaminar initial EMI value of 80dB was 33% higher than the control specimen. This specimen saw a reduction of almost 15% percent after 1 million cycles were applied. This configuration was able to withstand 23 times more cycles than the exterior configuration, almost 20 times more cycles than the midplane configuration, and almost 3 times more cycles than the control configuration. Its 68dB final value was 36% higher than the control's final value. It is clear that by adding nickel nanostrands™ the protection of the material was kept, while the control specimen was not able to provide a sufficient EMI protection level. Also the midplane configuration seemed to be the configuration with nickel nanostrands™ that offered the least amount of protection. Figure 30 shows an EMI comparison for the 75% UTS level. Figure 31 shows the normalized EMI values for the 75% UTS level.

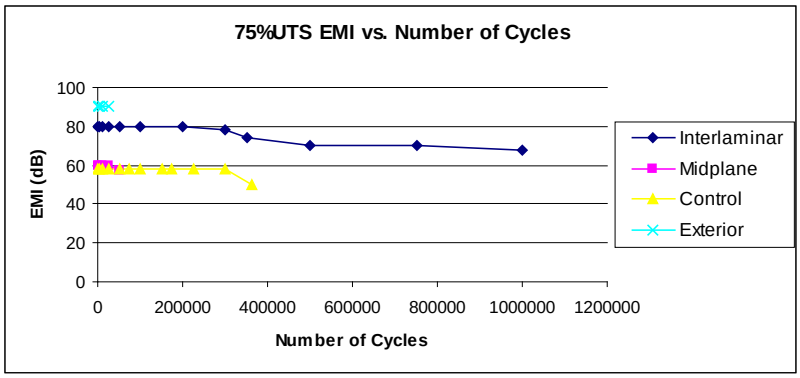

(a)

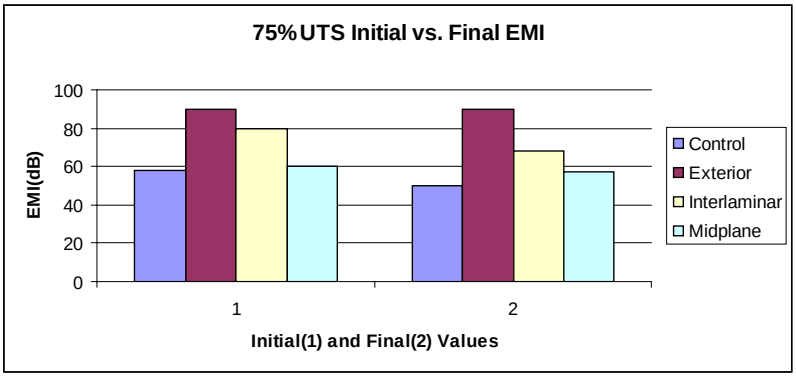

(b)

Figure 30. (a)EMI vs. No. of Cycles (b) Initial vs. Final Values for 75% UTS Level

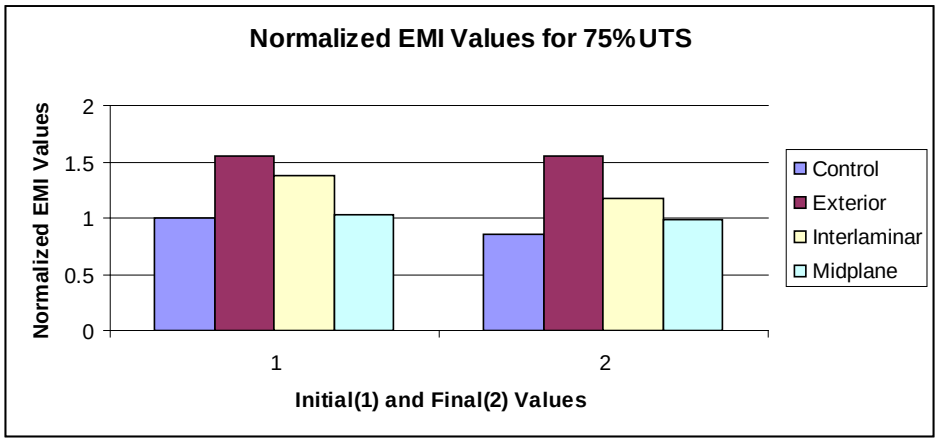

Figure 31. Normalized Resistance Values for 75% UTS Level.

4.3.3 EMI for 90% UTS Level

The EMI value for the control specimen remained constant throughout the test. This configuration was only able to withstand 27,470 cycles, less than 8% of its capability at 75%UTS and less than 2% of the applied amount at 60%UTS. A change in the EMI value for the midplane specimen was not able to capture during this test, due to failure after just 13 cycles were applied. This number represents less than 0.03% of its capability at 75%UTS and less than 0.0007% of the applied amount at 60%UTS. Table 9 shows the EMI values for the 90% UTS Level.

Table 9. EMI for 90% UTS Level

	Control	Exterior	Interlaminar	Midplane
	36.72 MPa to 367.2 MPa	42.75 MPa to 427.5 MPa	37.26 MPa to 372.6 MPa	45 MPa to 450 MPa
	(5.31 ksi to 53.1 ksi)	(6.21 ksi to 62.1 ksi)	(5.4 ksi to 54 ksi)	(6.525 ksi to 65.25 ksi)
Total # of Cycles	EMI (dB)	EMI (dB)	EMI (dB)	EMI (dB)
0	57	90	80	59
10,000	57	90	80	Failed @13 cycles
25,000	57	90	Failed @11300 cycles	
50,000	Failed @ 27,470 cycles	90		
100,000		90		
225,000		90		

The exterior configuration had the highest initial EMI value and kept its EMI value unchanged after 225,000 cycles were applied. Its final EMI value was 58% higher than the control's initial and final value. We need to remember that the 90%UTS exterior specimen experienced stress levels of 6.21 ksi to 62.1 ksi. The stress levels corresponded for 90% UTS on the 0.1016 panel, making the applied stress values less than a 90% UTS level for this thicker specimen.

The interlaminar configuration also kept its EMI values constant up to fracture. The interlaminar initial EMI value of 80dB was 40% higher than the control's initial and final value. The plotted data illustrates that at the end of the test all configurations containing nickel nanostrands™ performed better than the control specimen, as shown in Figure 32. Initial and final EMI values for 90% UTS stress level were normalized to observe how the EMI changes in all configurations contrasted to the initial value of the control specimen. Figure 33 shows the normalized EMI values for 90% UTS stress level.

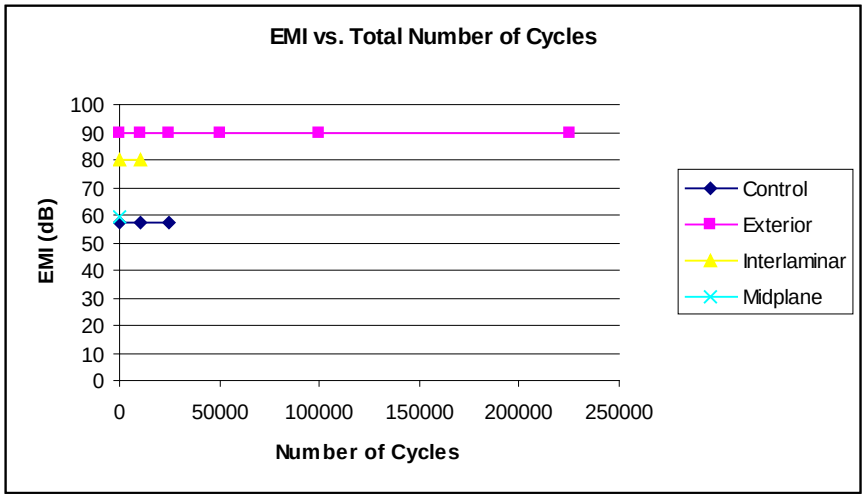

(a)

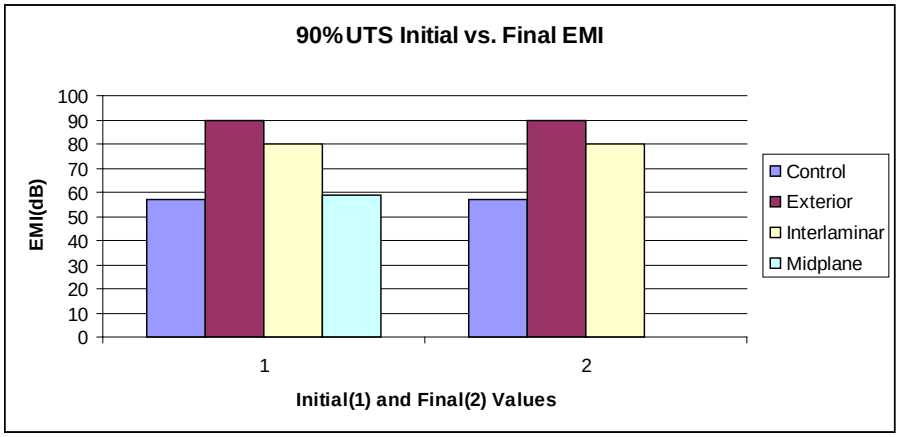

(b)

Figure 32. (a)EMI vs. No. of Cycles, (b) Initial vs. Final Values for 90% UTS Level

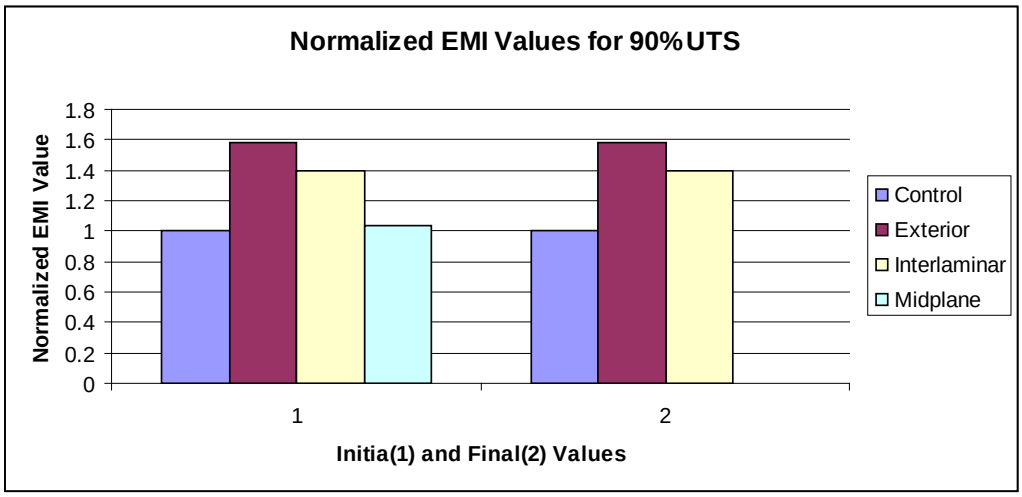

Figure 33. Normalized EMI Results for 90% UTS Level

4.4 Fatigue Testing

Specimens were inspected for failure mechanisms using an optical microscope (OM) and a Scanning Electron Microscope (SEM). Failures found during inspection were similar among the specimens, which consisted mainly of delamination and matrix cracking between the different layers. A common failure for most specimens under cyclic load was the development of delamination between the 90° and 0° plies, near the free edge as show in Figure 29. Also, delamination between the 90° and 45° plies and between the 45° and -45° plies was observed in most cases as the 75% UTS midplane specimen shown in Figure 34.

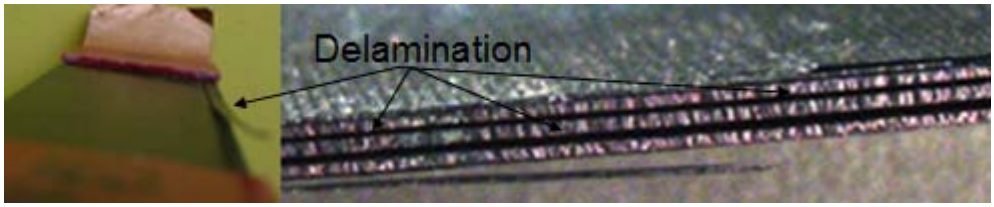

Figure 34. Delamination

Delamination between the 90° and 0° plies was the result of the stress concentration. The type of failure mechanism depends essentially on the layup of the material, and the type of loading. For laminates that have off-axis plies like the M55J/RS3 with stacking sequence $[0, 90, +\text{-}45]_S$, the first and most profuse damage mode is matrix cracking. During cyclic loading, cracks formed through the thickness of the plies, aligned parallel to the fiber direction and perpendicular to the to the 0° ply, initiating damage in the 90° ply. This damage resulted in delamination between the 0° and 90° plies. It was observed that the delamination was constrained to grow between individual plies, along the entire length of the specimen. Another general observation in the specimens that completely broke was the fact that the initial damage caused by the 90° ply developed in more delamination between the damaged 90° ply and the 45° ply. This delamination kept growing causing the 45° and -45° plies to also delaminate, resulting in shear failure of the specimens.

4.4.1 Fatigue Testing – 60% UTS

At this stress level none of the 4 configurations completely fracture as shown in Figure 35. Most of the specimens suffered extensive delamination and matrix cracking but none of them separated in 2 or more pieces after 2 million cycles were applied.

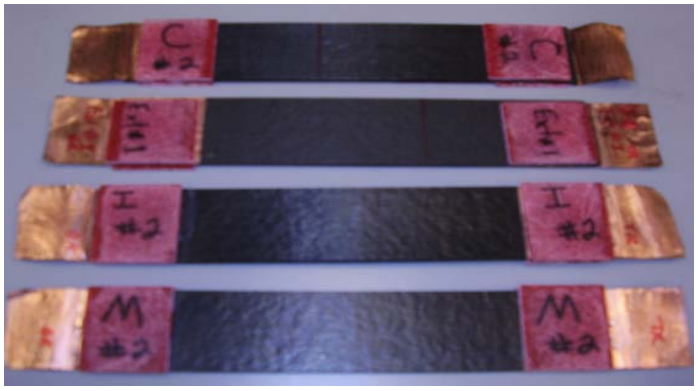

Figure 35. 60% UTS Test Specimens

The control specimen suffered delamination between the 0° and 90° plies, between 90° and 45° plies, and between the 45° and -45°, in different areas along the length of the specimen. Figure 36 also shows both sides of the control specimen. A closer look of a damaged area is presented in Figure 37, where delamination and matrix cracking is clearly seen.

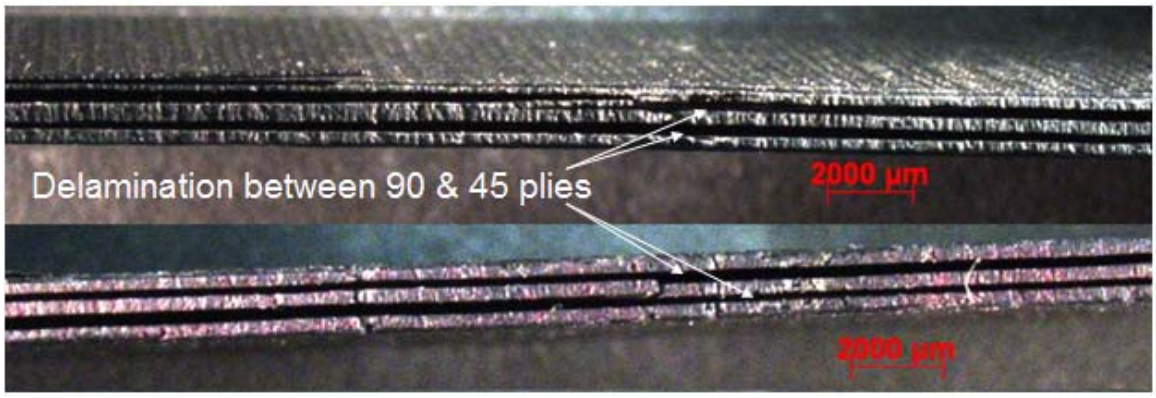

Figure 36. 60% UTS Control Specimen

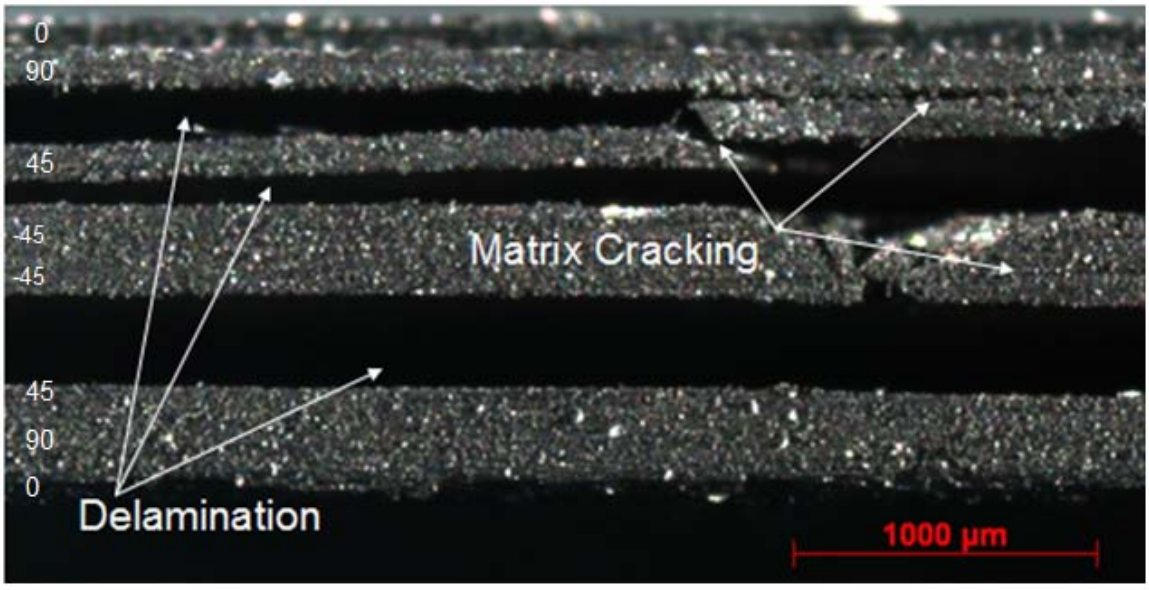

Figure 37. 60% UTS Control Specimen

The exterior specimen similar to the control specimen suffered delamination between the 0° and 90° plies, between 90° and 45° plies, and between the 45° and -45°, in different areas along the length specimen as shown in Figure 38. A closer look of a damaged area is presented in Figure 39, where delamination and matrix cracking is seen.

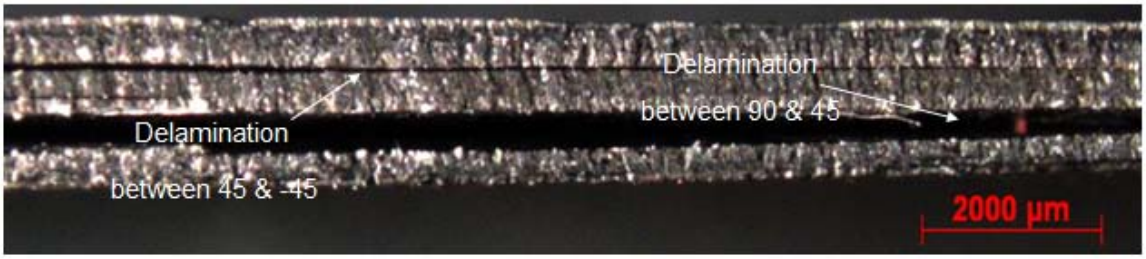

Figure 38. 60% UTS Exterior Specimen

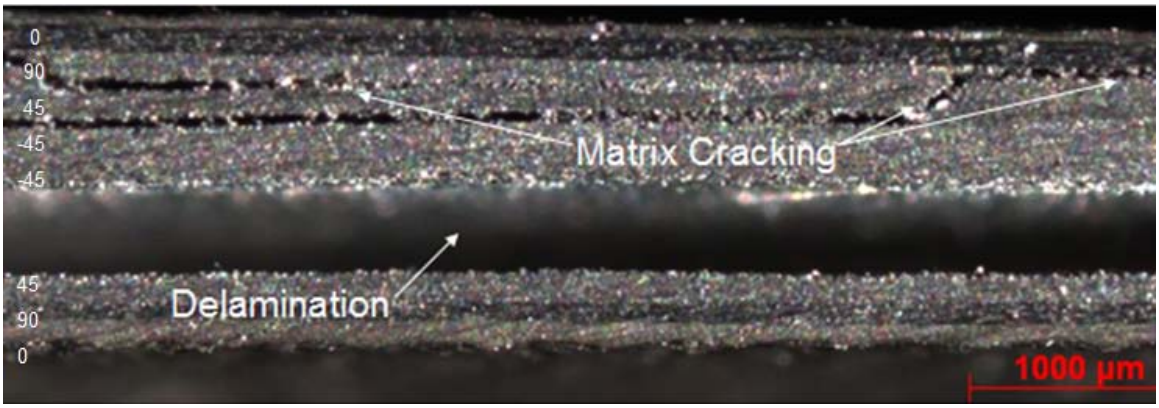

Figure 39. 60% UTS Exterior Specimen

For the interlaminar specimen its delamination concentrated more between the 90° and 45° plies as shown in Figure 40. No delamination or matrix cracking was observed across the nanostrands layer. Up to this point the nanostrands layer didn't seem to be affected by the cyclic loading, and were still protecting the material. Sand paper was used to polish the surface in order to find damage that wasn't detected previously, but no new damage was observed on any of the sides of the specimen. A closer look of a damaged area is presented in Figure 41, where delamination is seen.

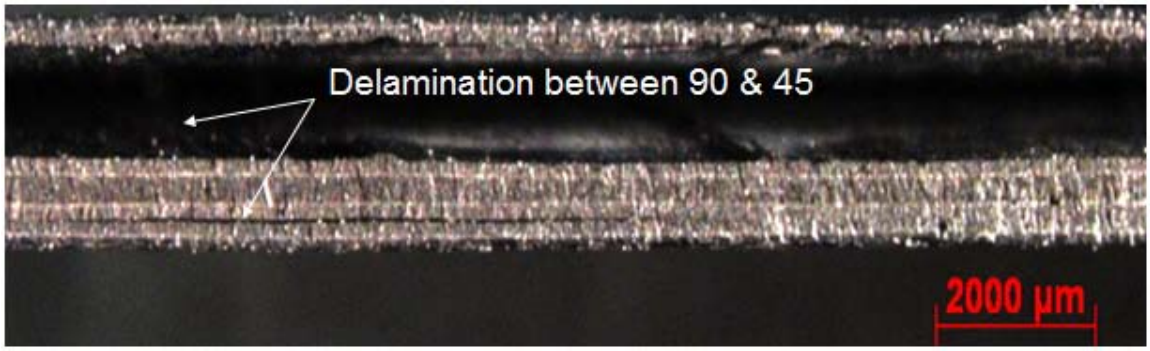

Figure 40. 60% UTS Interlaminar Specimen

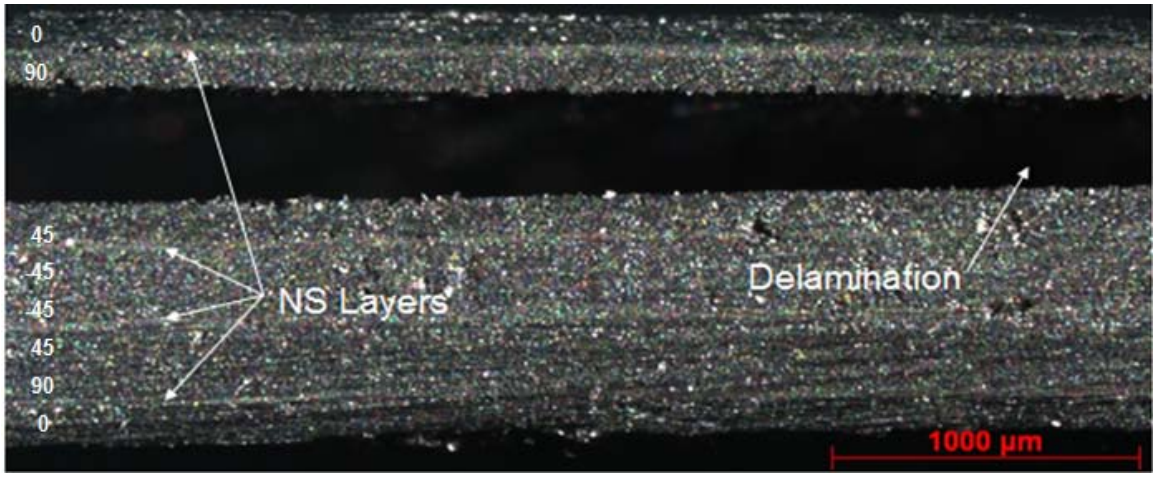

Figure 41. 60% UTS Interlaminar Specimen

For the midplane specimen no major delamination was detected. Sand paper was used to polish the surface in order to find damage that wasn't detected previously, but no new damage was observed on any of the sides of the specimen. Up to this point any matrix cracking or delamination did not surfaced yet. In Figure 42 the nanostrands™ layer seemed to be intact. A closer look of a damaged area is presented in Figure 43.

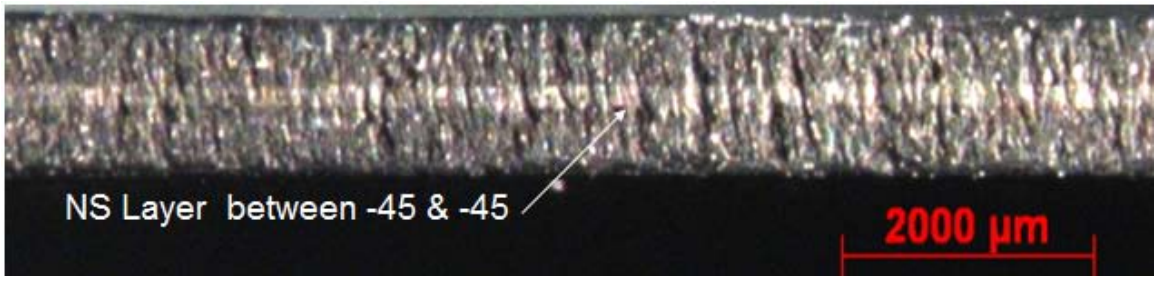

Figure 42. 60% UTS Midplane Specimen

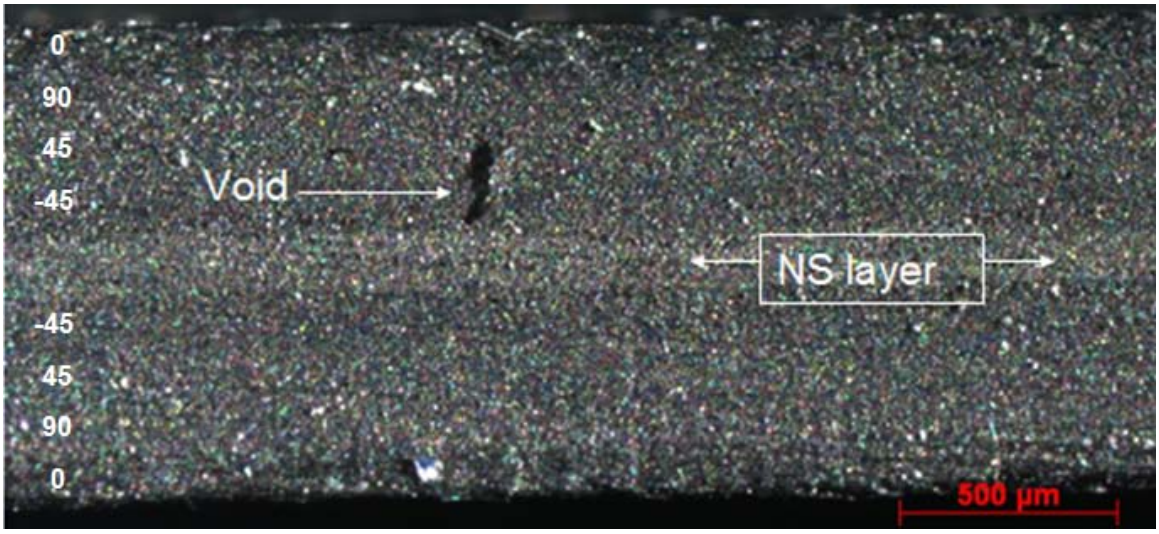

Figure 43. 60% UTS Midplane Specimen

4.4.2 Fatigue Testing – 75% UTS

At this stress level the control and exterior configurations, completely fractured. The midplane configuration sustained massive delamination and matrix cracking, but didn't fracture. The interlaminar specimen suffered delamination and matrix cracking, but was less damaged than any of the other configurations. The control specimen suffered delamination between the 0° and 90° plies, between 90°and 45° plies, and between the 45° and -45°, in different areas along the length specimen. Shear failure of the specimen

was observed as shown in Figure 44. A closer look to the shear failure area is presented in Figure 45.

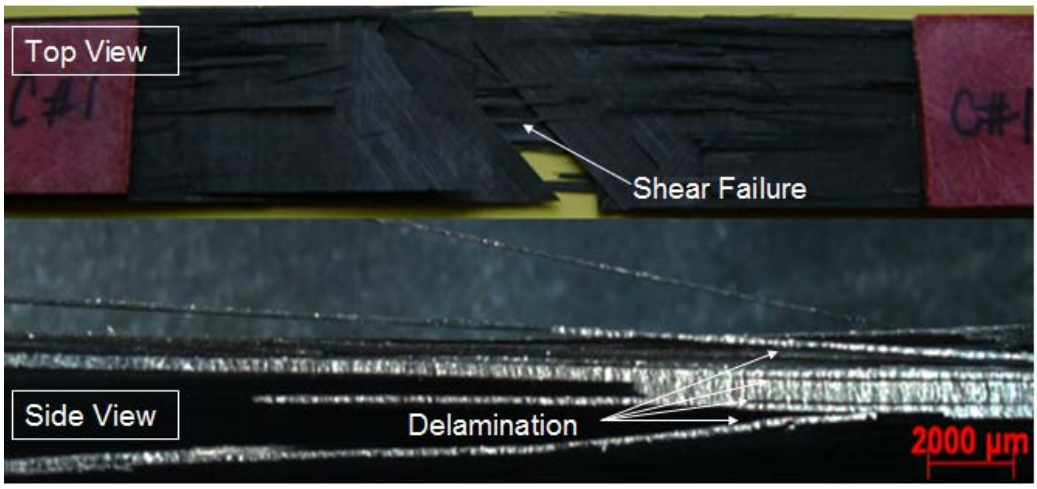

Figure 44. 75% UTS Control Specimen

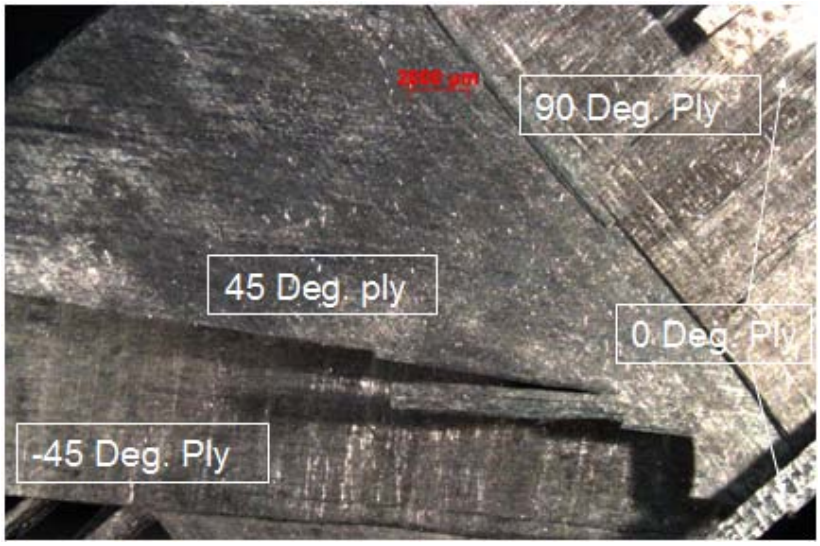

Figure 45. 75% UTS Control Specimen

Because all M55J/RS3 specimens had the same stacking sequence $[0, 90, +\text{-}45]_S$, the damage generated by cyclic loading originated in the same manner, cracks formed through the thickness of the plies, aligned parallel to the fiber direction and perpendicular

to the to the 0° ply, initiating damage in the 90° ply. The exterior specimen suffered delamination between the 0° and 90° plies, between 90° and 45° plies, and between the 45° and -45°, in different areas along the length specimen, but constrained its grow between individual plies. Shear failure of the specimen was observed as shown in Figure 46. Figure 47 shows the damaged stacking sequence. A closer look in Figures 48a and 48b shows delamination and the condition of nickel nanostrands after fracture.

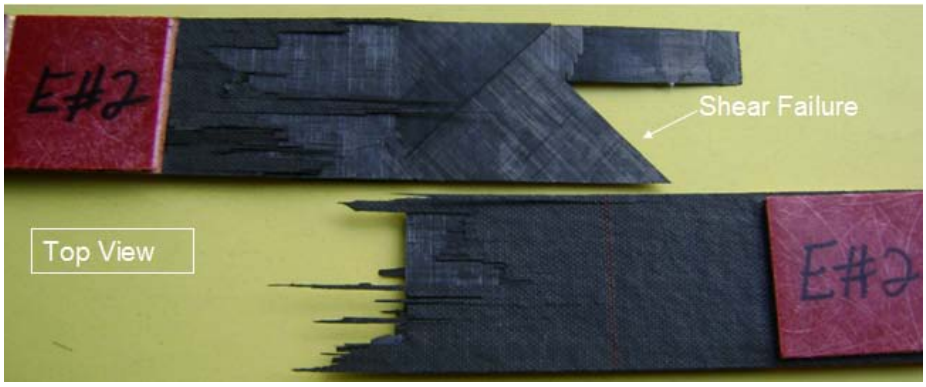

Figure 46. 75% UTS Exterior Specimen

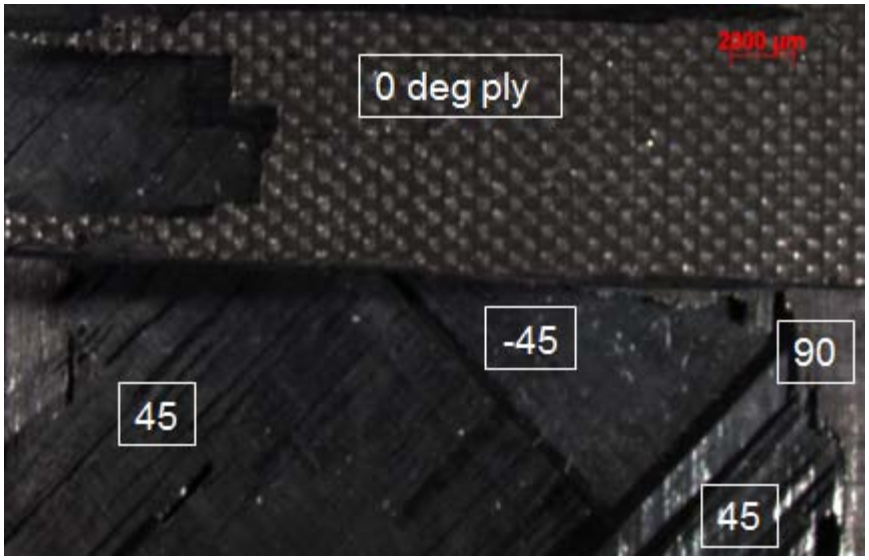

Figure 47. 75% UTS Exterior Specimen

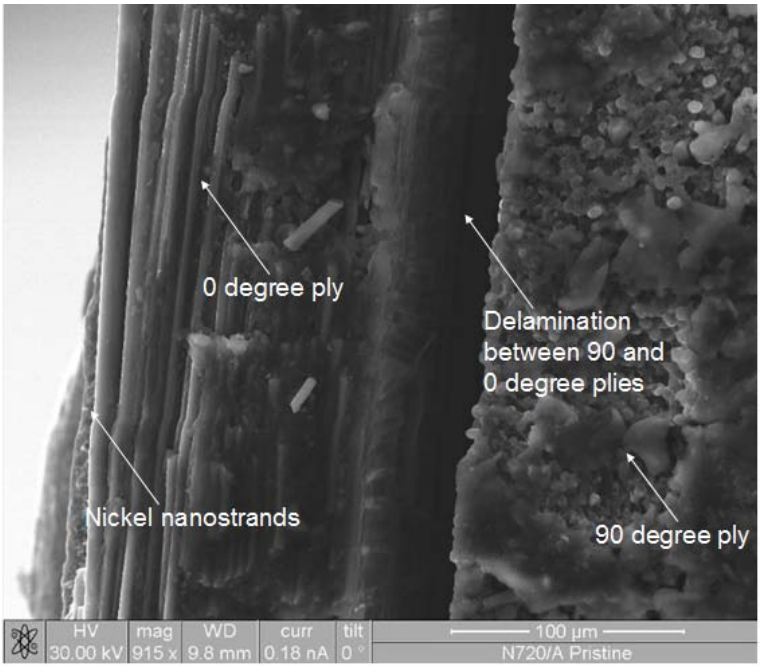

Figure 48.a. SEM-75% UTS Exterior Specimen

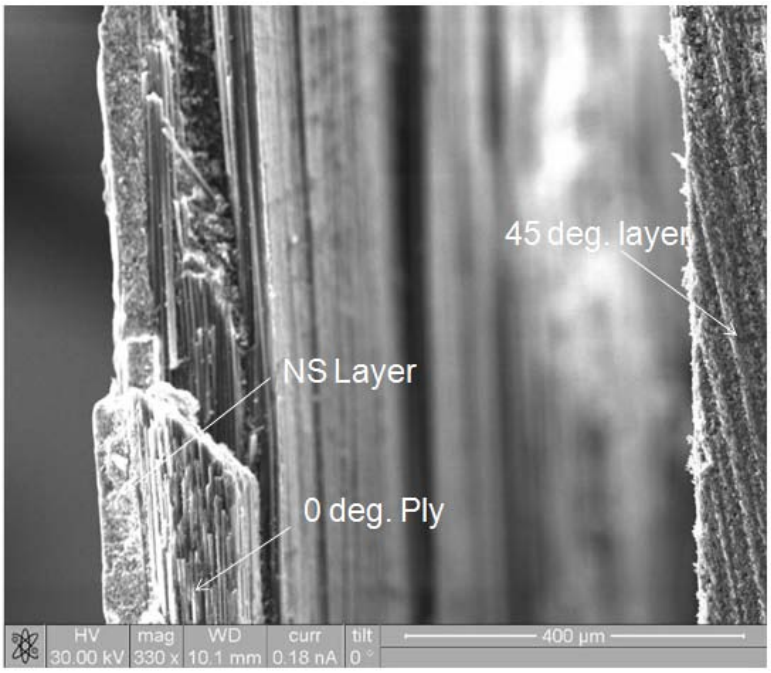

Figure 48.b. SEM-75% UTS Exterior Specimen

For the interlaminar specimen shown in Figure 49, as in the 60%UTS level, its delamination concentrated more between the 90° and 45° plies. Also, the 0° ply started to visibly crack after 1 million of cycles were applied. A closer look to the side of the specimen is presented in Figures 49 to 51, where delamination between the 90° and 45° plies is clearly seen. Figures 50 and 51 show how cracks propagated along the nickel nanostrands™ layers without crossing or affecting them. Figure 52 shows a closer look of the area between the nickel nanostrands™ layer and the -45° ply. Upon inspection, the nickel nanostrands™ area seemed to be intact.

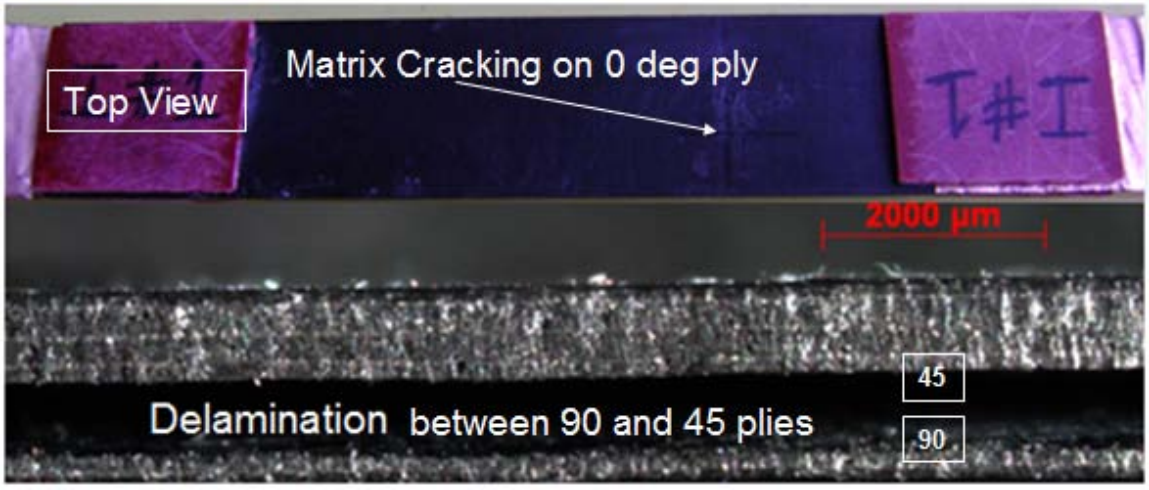

Figure 49. 75% UTS Interlaminar Specimen

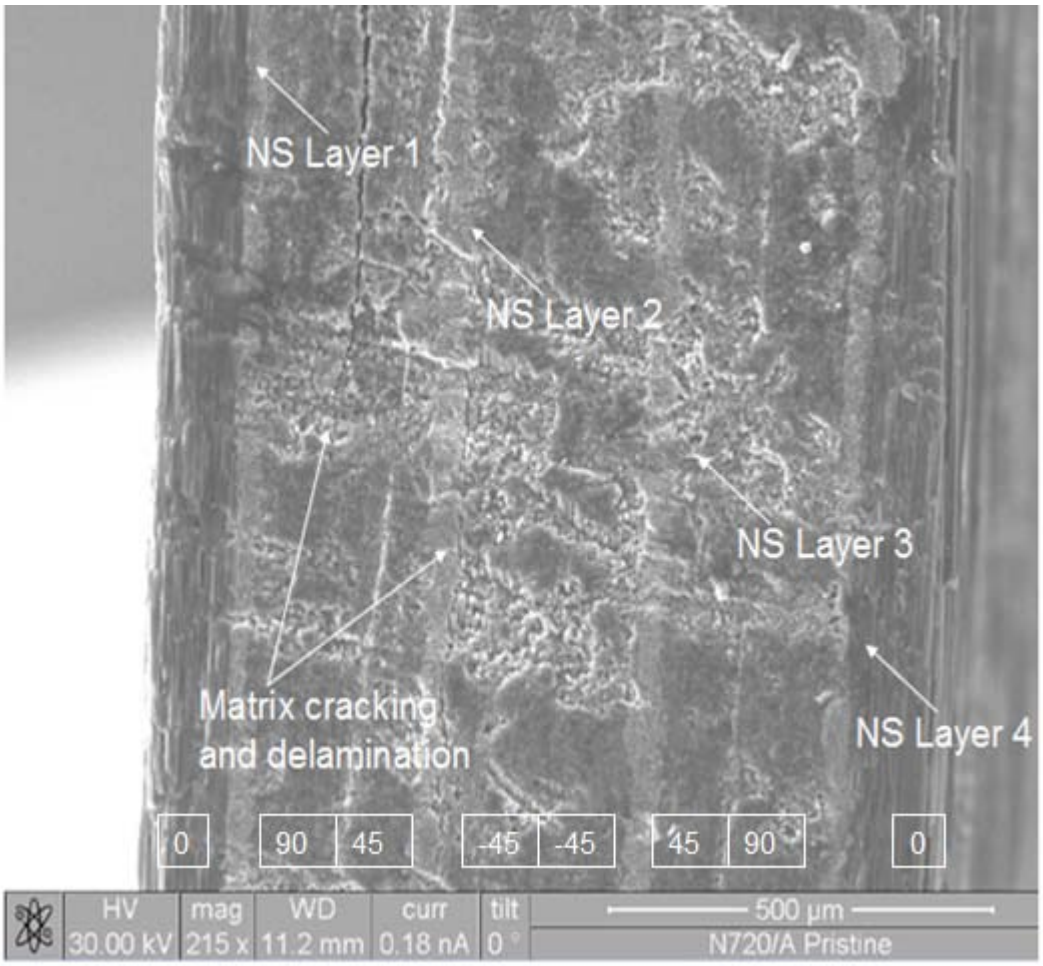

Figure 50. SEM-75% UTS Interlaminar Specimen

Figure 51. SEM-75% UTS Interlaminar Specimen

Figure 52. SEM-75% UTS Interlaminar Specimen

As previously mentioned, the midplane configuration sustained massive delamination and matrix cracking as show in Figure 53. The specimen almost fractured, but it was interesting to see that the damage in this specimen occurred above and below the nanostrands layer, but not across the layer as shown in Figure 54. All plies have suffered extensive damaged, but the nanostrands layer was mostly unaffected. In addition to still be providing the required protection, the nanostrands layer might be acting as a barrier that deflects matrix cracking. Upon inspection, the nickel nanostrands^{TM} area seemed to be intact.

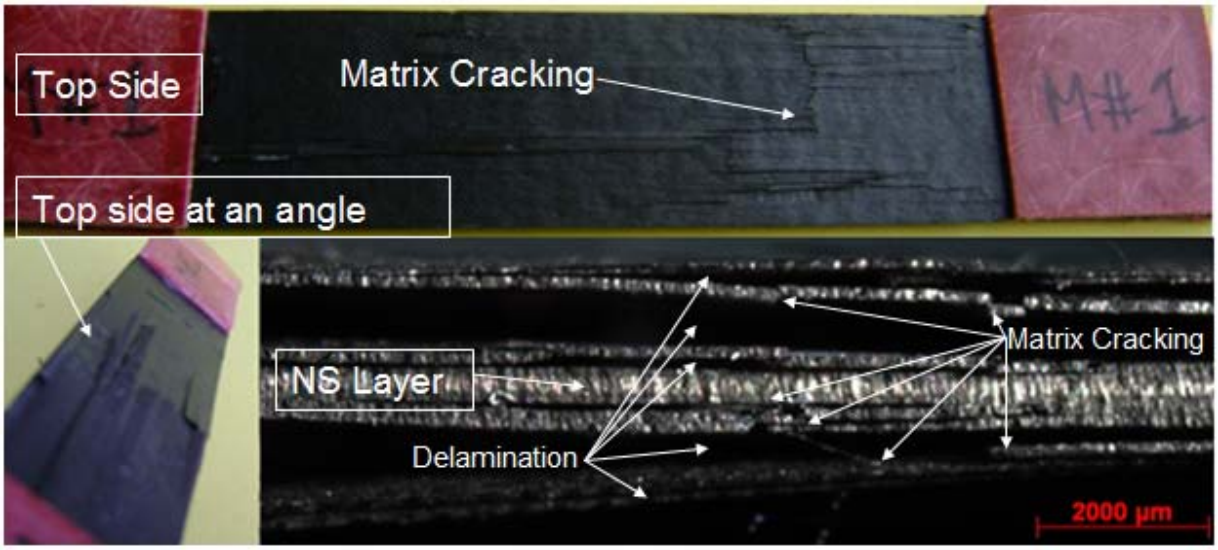

Figure 53. 75% UTS Midplane Specimen

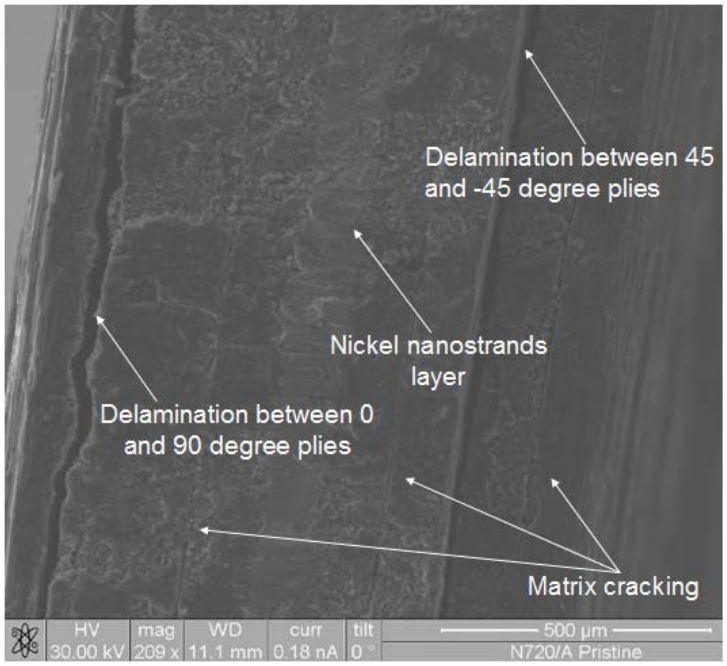

Figure 54.a. SEM-75% UTS Midplane Specimen

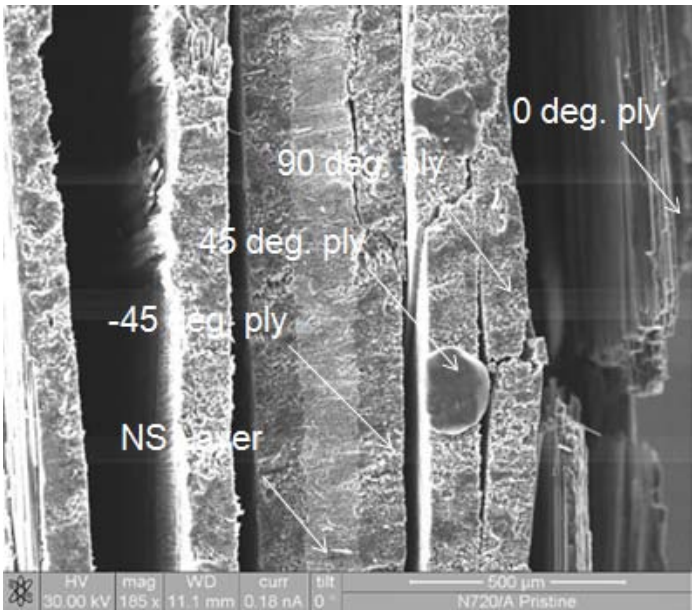

Figure 54.b. SEM-75% UTS Midplane Specimen

4.4.3 Fatigue Testing - 90%UTS

In this stress level the control configuration completely fractured. Failure mode was the same as in the previous stress levels due to the M55J/RS3 specimens' stacking sequence. The damage generated by cyclic loading initiated in the 90° ply, causing delamination between the 0° and 90° plies, between 90° and 45° plies, and between the 45° and -45°, finally causing shear failure of the control specimen. Shear failure of the specimen was observed as shown in Figure 55. The damage was so severe that the lower and upper surfaces were almost completely destroyed.

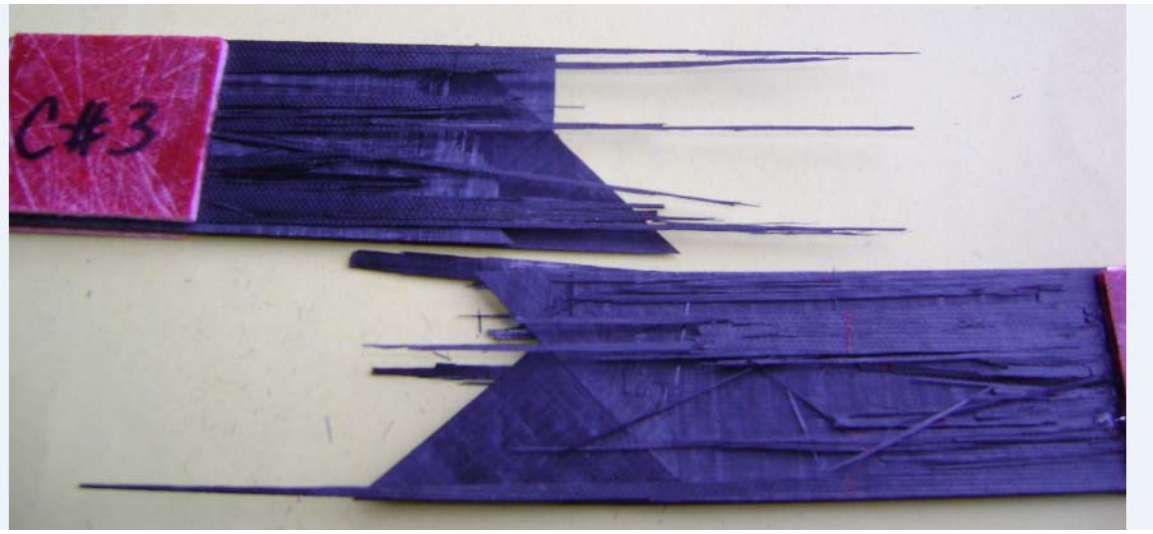

Figure 55. Control Specimen for 90% UTS Level

The midplane configuration sustained massive delamination and matrix cracking and almost fractured. The midplane specimen suffered damaged but not as severe as the control configuration. The midplane specimen suffered delamination between the 0 and 90° plies, , and between 90° and 45° plies, in different areas along the length specimen. Figure 56 shows delamination and matrix cracking.

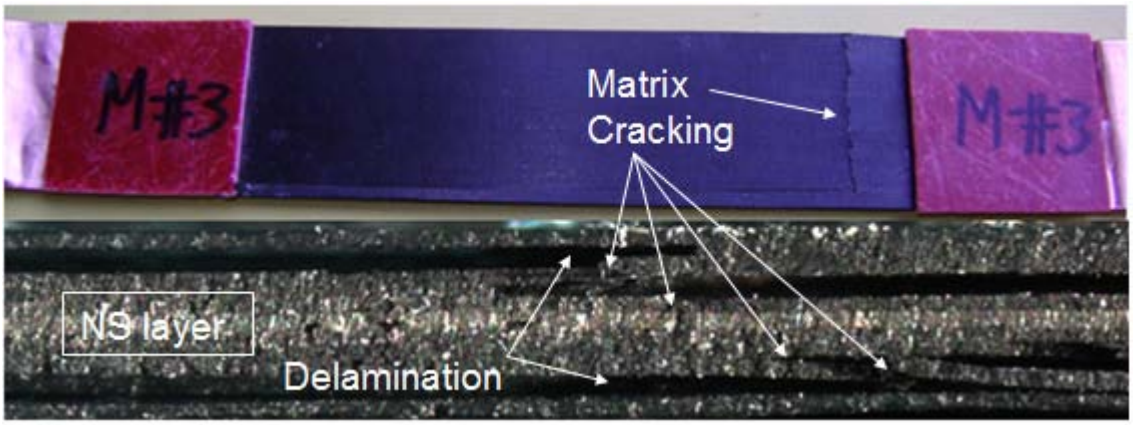

Figure 56. Midplane Specimen for 90% UTS Level

The interlaminar configuration sustained massive delamination and matrix cracking and almost fractured. The interlaminar specimen suffered damaged but not as severe as the control configuration, concentrating its delamination between the 90 and 45 plies, along the length specimen. Figure 57 shows the delamination.

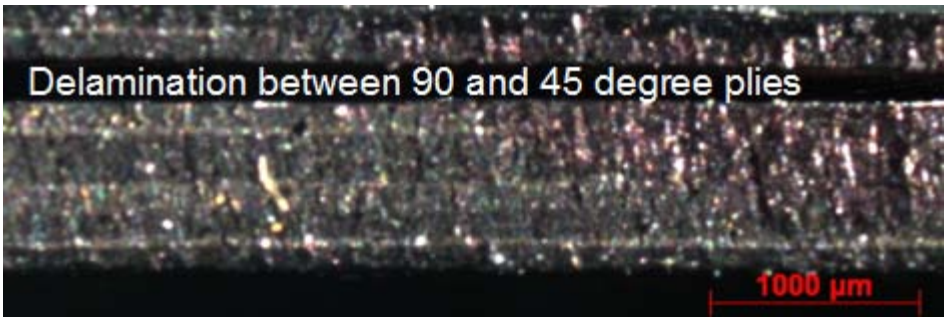

Figure 57. Interlaminar Specimen for 90% UTS Level

The exterior specimen was the one that was able to sustain the most amount of cycles. This configuration suffered matrix cracking and delamination between the 0 and 90° plies, and between 90° and 45° plies, in different areas along the length specimen as shown in Figure 58.

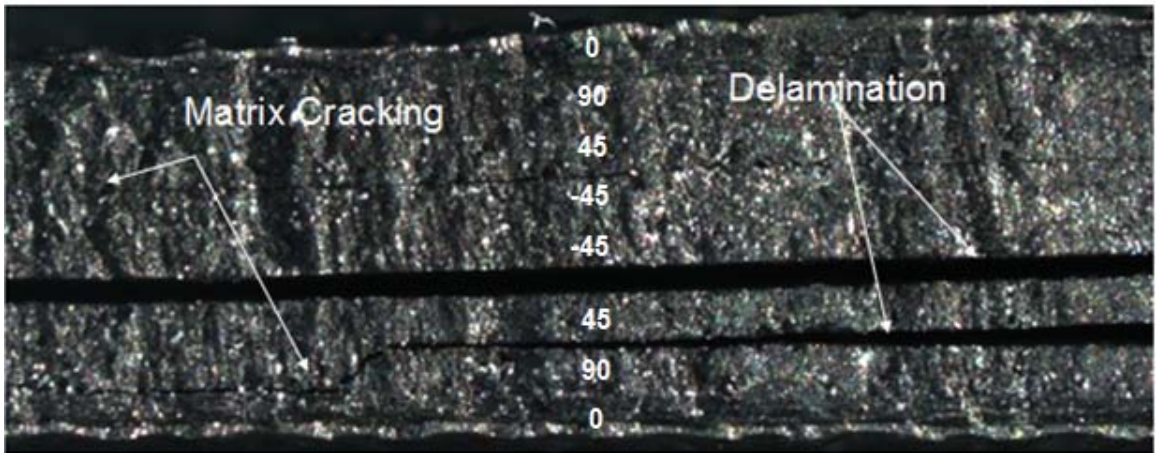

Figure 58. Exterior Specimen for 90% UTS Level

4.5 Number of Cycles vs. Stress Levels

The data gathered relating the number of cycles during the test is shown in Table 10. Two million cycles were applied to all specimens at a 60%UTS level without causing fracture. When the stress level was increased to 75% the interlaminar specimen was able to withstand the most amount of cycles. At 90% UTS the exterior specimen was able to withstand the most amount of cycles. There are many variables that could have influenced the results such as manufacturing flaws, induced faults during fabrication of specimens and errors in the test procedure are some of them. An important note to make is that the specimen used for the 90%UTS was thicker than the other specimens. As a result, the load applied to was lower than 90%UTS, explaining why this specimen was able to withstand more cycles. Also, a bigger sample size will definitely help to reduce the influence of imperfections and mistakes. Figure 59 shows how the stress levels affected the number of cycles that each configuration was able to withstand.

Table 10. Number of Cycles vs. Stress Levels

Configuration - Stress Level	Cycles experienced
Control - 60% UTS 24.28 MPa to 244.8 MPa (3.54 ksi to 35.4 ksi)	2,000,000
Exterior - 60% UTS 28.5 MPa to 285 MPa (4.14 ksi to 41.4 ksi)	2,000,000
Midplane - 60% UTS 30 MPa to 300 MPa (4.35 ksi to 43.5 ksi)	2,000,000
Interlaminar - 60% UTS 24.84 MPa to 248.4 MPa (3.6 ksi to 36 ksi)	1,500,000
Control - 75% UTS 30.6 MPa to 306 MPa (4.425 ksi to 44.25 ksi)	366,000
Exterior - 75% UTS 35.63 MPa to 356.3 MPa (5.175 ksi to 51.75 ksi)	43,000
Midplane - 75% UTS 37.5 MPa to 375 MPa (5.438 ksi to 54.38 ksi)	50,300
Interlaminar - 75% UTS 31.05 MPa to 310.5 MPa (4.5 ksi to 45 ksi)	1,000,000
Control - 90% UTS 36.72 MPa to 367.2 MPa (5.31 ksi to 53.1 ksi)	27,470
Exterior - 90% UTS 42.75 MPa to 427.5 MPa (6.21 ksi to 62.1 ksi)	225,000
Midplane - 90% UTS 45 MPa to 450 MPa (6.525 ksi to 65.25 ksi)	13
Interlaminar - 90% UTS 37.26 MPa to 372.6 MPa (5.4 ksi to 54 ksi)	11,300

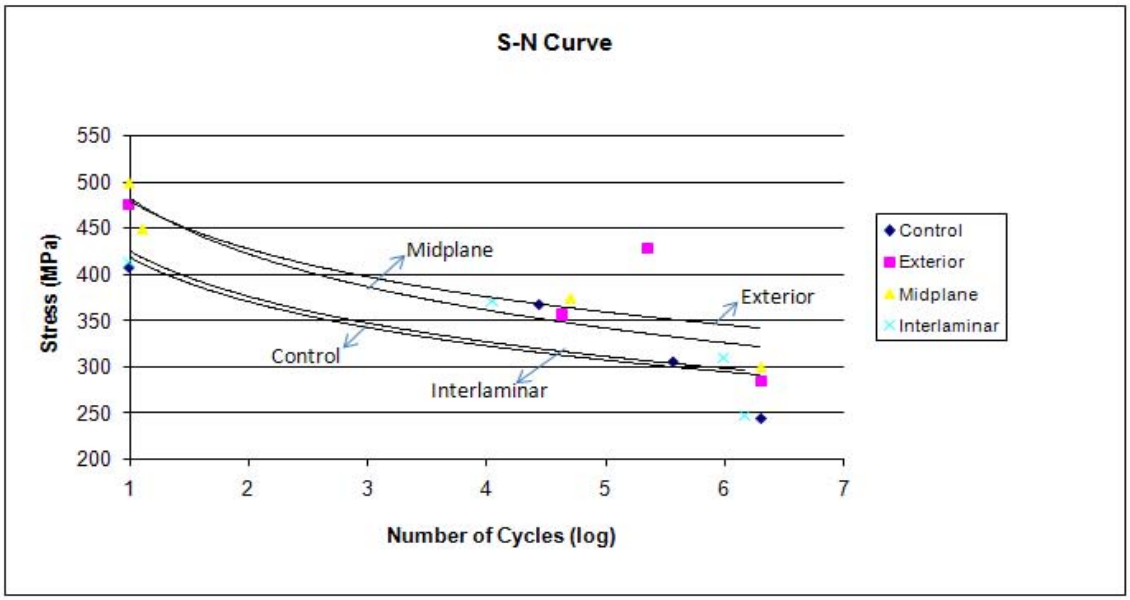

Figure 59. Number of Cycles vs. Stress Levels

V. Conclusions and Recommendations

This chapter begins with a summary of the research conducted on, followed by conclusions drawn based on the test data analysis. Suggestions for future work are presented at the end.

5.1 Summary

In this research effort we investigated the changes in the electrical properties of 4 configurations of the M55J/RS3 material while it was subjected to a series of cycles and cyclic stress levels (fatigue load). Resistance & EMI measurements were taken before and after each fatigue load to record the change in their properties. All 4 configurations consisted of a symmetric 4 plies layup of M55J/RS3 composite material with its fibers oriented at 0/90/45/-45 degrees. The Control configuration had no nickel nanostrands™, and the remaining three configurations (exterior, midplane and interlaminar) had nickel nanostrands™ added in different location of the material. Existing composite materials don't have the electrical properties to protect satellites from radiation and other harsh conditions. Current space systems require the addition of metal shields in order to function in space. The addition of nickel nanostrands™ layers has the objective of combining the attributes of nanocomposite structures with the electrical traits of metal materials in order to provide the conduction and electromagnetic shielding needed to successfully operate satellites in space.

5.2. Conclusions

Analysis of the test data resulted in the following conclusions:

A. Effect of tension-tension cyclic loading on specimens resistance

- The application of tension-tension cyclic loading resulted in an increase in the resistance values of all configurations at all tested stress levels. Of all configurations the exterior configuration had the best performance having the lowest initial and final resistance values for all stress levels. The excellent performance by the exterior configuration is due to its capacity to conduct the electric charge along the surface without going through the material. Nickel nanostrands^{TM} in the interlaminar and midplane configurations resulted in lower final values than the control specimen.
- The results obtained for the 60%UTS level showed the control specimen increased 38%, the exterior configuration increased 10%, the interlaminar increased 6%, and the midplane configuration increased 9%. At the 75%UTS level the control specimen and interlaminar configurations doubled its initial value, and the exterior and midplane configurations increased 7% and 20% respectively. The 90% UTS level increased the resistance of the control, interlaminar and midplane specimens at a faster rate. The exterior specimen had a relative constant response.
- The exterior configuration performed better followed by the interlaminar, midplane, and control configurations. Even after two million cycles the initial resistance value for the interlaminar and midplane configurations was higher than the final values of the exterior specimens.

B. Effect of tension-tension cyclic loading on EMI shielding protection

- The application of tension-tension cycling loading did not affect greatly the EMI shielding protection of the configurations with nickel nanostrands™. Of all four configurations, the exterior configuration had the highest initial EMI value of 90 dB. The nickel nanostrands™ provided an initial value that was 50% higher than the initial value of the control specimen. The exterior specimen kept its EMI value almost unchanged at all stress levels.
- The interlaminar and midplane configurations also kept their EMI values practically constant. The interlaminar configuration offered a higher protection than the midplane, but on both configurations the nickel nanostrands™ were effective in providing the required EMI protection.
- The control specimen offered the lowest EMI protection. This configuration was the most affected with the addition of cyclic loads.

C. Failure mechanisms

- An increase in stress level caused a decrease in the amount of cycles experienced on all specimens. Midplane and Exterior configurations failed sooner than the control during the 75%UTS level at less than 3% of the amount of cycles applied at 60%UTS.
- The location of the nickel nanostrands™ seemed to affect crack propagation. The interlaminar configuration seemed to have less damage during the 60% and 75% UTS level and was able to withstand the most amount of cycles for the 75%UTS. Nickel nanostrands™ between the 0°

and 90° laminates and between the 45° and -45° laminates might have acted as a barrier against crack propagation.

- In all configurations the initial damage occurred in the 90 ° ply, the weakest ply in the stacking sequence. Delamination developed between the 90° ply and the 45°. Transverse stresses caused the 0° to experience matrix cracking and delamination.
- Inspection of specimens using an SEM showed that the nickel nanostrands™ layers remained almost intact up to fracture. In addition, the nanostrands™ layer might be acting as a barrier that deflects matrix cracking, while maintaining the required protection.

5.3 Recommendations for Future Work

This research effort was a small undertaking in the research of nanocomposites as lightweight electronic enclosures for satellites' applications. A similar study using different metallic nanostrands is necessary to compare and determine the best material solution. Nickel nanostrands™ between the 0° and 90° laminates and between the 45° and -45° laminates might have acted as a barrier against crack propagation during our study. A study of the influence of nickel nanostrands™ in the composites' fracture mechanics will expand the knowledge on the M55J/RS-3 configurations attributes and capabilities, and will contribute in finding the alternative for lightweight nanocomposite to be used for satellites applications.

Appendix A.

MTS Testing Sequence

- *Open Station Manager and select Configuration File (need to create one initially).*

- *Select Function Generator*
  - *To warm up machine (in displacement control mode)*
  - *Target set point*
  - *To apply hydraulics (in order to move grips up or down)*

    - *Push Reset*
    - *Push Low power*
    - *Push High power*

  - *To Adjust Lower grip distance*
    - *Go to Station Control on Right side of window*
      - *Auto Offset*
      - *Detector*
      - *Manual command (specifies which mode we are in)*
        - *Find or refine/Adjustment/Use Arrows/gage*
      - *Control mode*
        - *Use displacement command as control mode*
      - *Active mode*
        - *Use force control*

  - *Warming up of the MTS machine avoids accumulation of residue particles in the line that may cause hydraulic pike.*
  - *Use square wave to warm up machine.*
    - *To warm up:*
      - *Click **RESET**/ HPU low power (wait for light) / HPU high power*
      - *Click Start, wait 30 minutes, then Click stop.*
  - *Procedure Editor*
    - *Count (each count is half a cycle)*

- *Go to :*
  - *MPT Procedure*

        - *Open Procedure*

    - *Data Collection*
        - *Put data collection in front of command*

    - *Data acquisition*
        - *Continuous sampling*
    - *Gather:*
        - *Force*
        - *Force Command*
        - *Displacement*
        - *Displacement Control*
        - *Strain*

- *Check: First Header Data Only*

- *Check: Process enable*

- *To Start testing*
    - ***Grip top part first.***
    - *Go to control mode (on displacement mode) – Menu Command Window*
    - *Go to signal Offset (to Zeroed)*
    - *Go from displacement mode to force mode*
    - *Menu command window type zero lb (or 0.0 kip).*

    - *Then grip lower part.*

    - *Run Procedure.*
        i. *Can't start test without uncheck manual command.*

    - *Unlock procedure at end of the test.*

    - ***Ungrip bottom part first.***

- *As soon as you ungrip bottom (in force mode)*
    i. *Change from force mode to displacement mode.*

- *Go to SPEC DATA to access files.*

Appendix B.

Additional Optical Microscope and SEM Photos

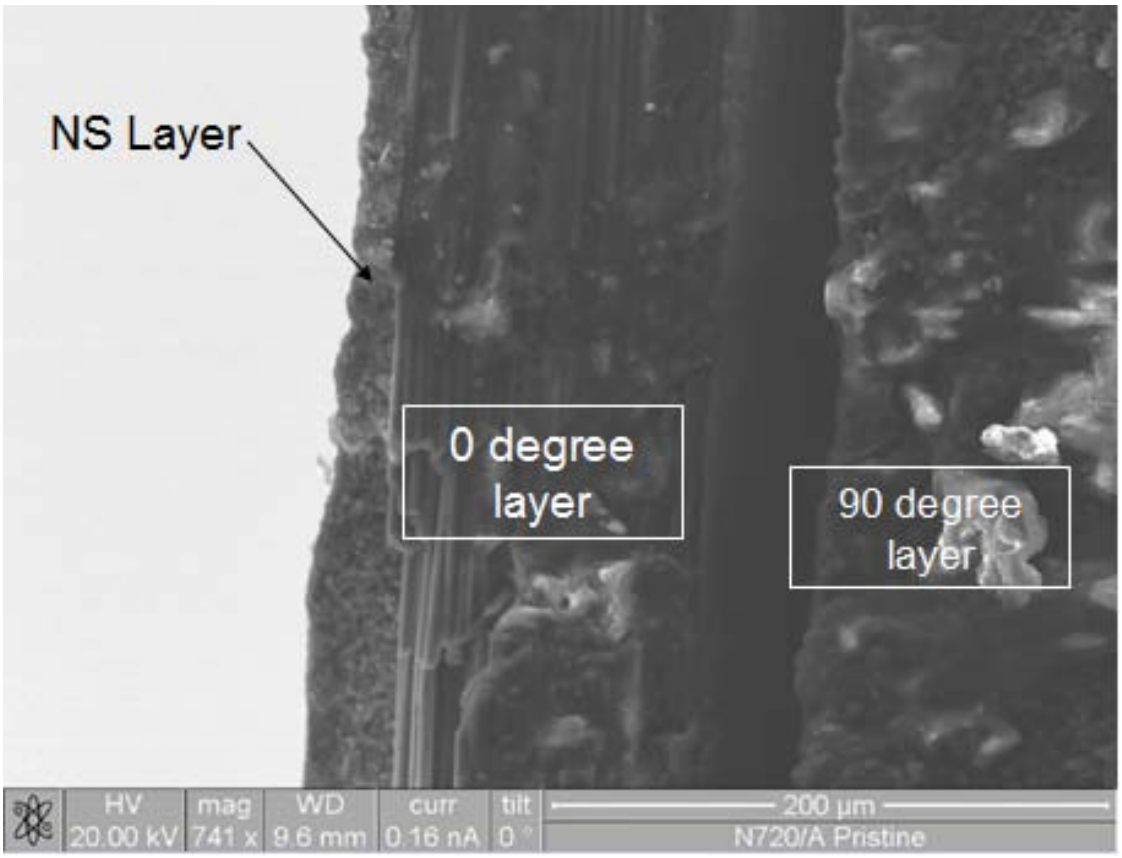

Figure 60. SEM-75% UTS Exterior Specimen

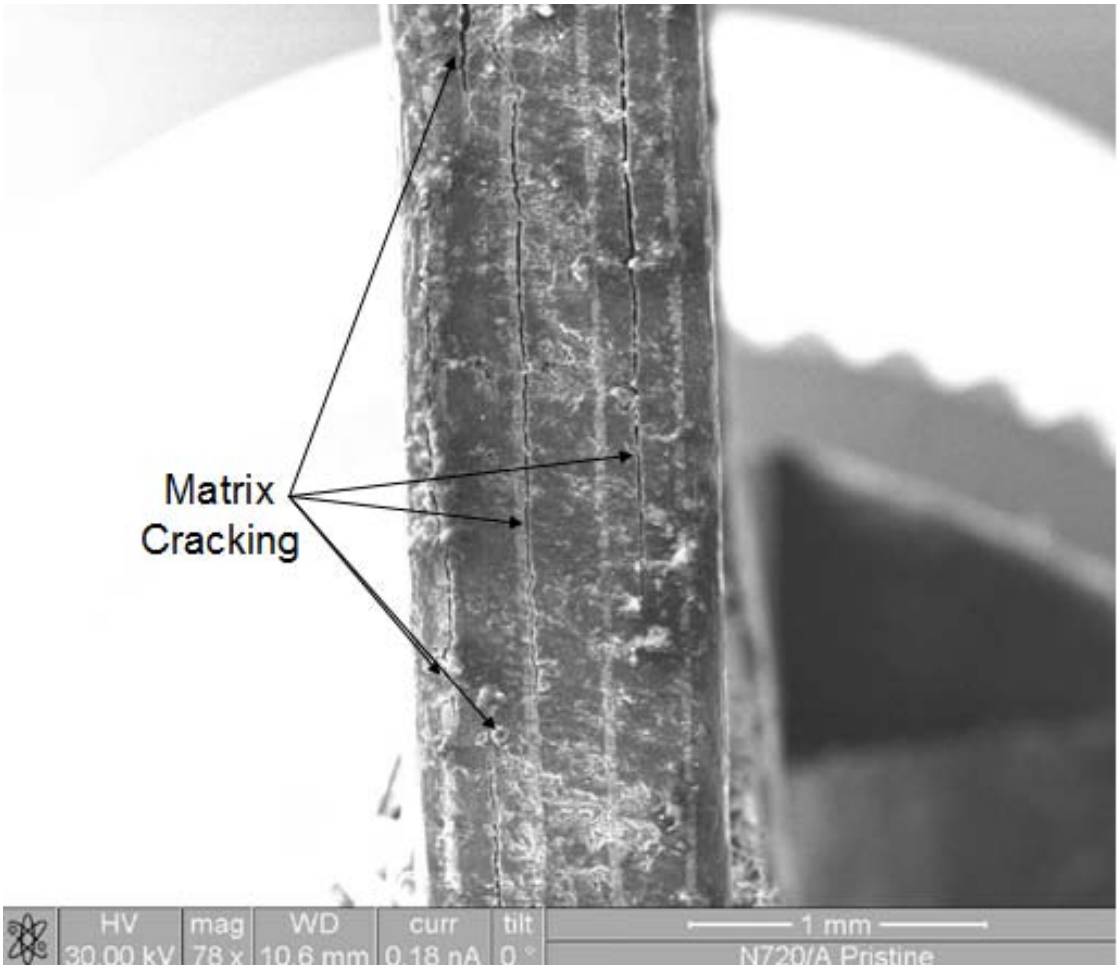

Figure 61. 75% UTS Interlaminar Specimen

Figure 62. 75% UTS Midplane Specimen

Bibliography

[1] G. Hansen, "High Aspect Ratio Sub-Micron and Nano-scale Metal Filaments," *SAMPE Journal,* vol. 41, 2005.

[2] D. D. Davis, G. F. Pezdirtz, L. Roberts, R. Kemp, and H. B. Probst , "Materials for Space Operations", *NASA – University Conference on the Science and Technology of Space Exploration,* 1962.

[3] N. E. Dowling, *Mechanical Behavior of Materials.* New Jersey: Prentice Hall, 2007.

[4] G. Harris, J. Lennhoff, J. Nassif, M. Vinciguerra, P. Rose, D. Jaworski and J. Gaier, "Lightweight Highly Conductive Composites for EMI Shielding," *SAMPE Journal.,* vol. 36, pp. 59-63, 2000.

[5] T. D. Damon, *Introduction to Space.* Florida: Krieger Publishing Company, 2001.

[6] C.T. Herakovich, *Mechanics of Fibrous Composites*. New York: John Wiley & Sons, 1998.

[7] G. Benedek, P. Milani, V.G. Ralchenko, *Nanostructured Carbon for Advanced Applications.* Netherlands: Kluwer Academic Publishers, 2001.

[8] M.J. O'Connell, *Carbon Nanotubes.* Florida: Taylor & Francis Group, 2006.

[9] G. Cao, *Nanostructures & Nanomaterials*. London: Imperial College Press, 2004.

[10] G.V.E. Thompson, K.W. Gatland, *Materials in Space Technology.* London: Ilifffe Books Ltd; 1963.

[11] J.W. Haffner, *Radiation and Shielding in Space.* New York: Academic Press Inc; 1967.

[12] National Aeronautics and Space Administration, "*Space Radiation Protection*". *NASA Reference Publication SP-8054,* 1970.

[13] NATO Advisory Group for Aerospace Research and Development, *Electromagnetic Effects of Carbon Composite Materials upon Avionics Systems.* AGARD Conference Preprint No. 283.

[14] T. Rikitate, *Magnetic and Electromagnetic Shielding.* Japan: Terra Scientific Publishing Co.; 1987.

[15] R. Tarija, *Damage Mechanics of Composite Materials*. Netherlands: Elsevier Science B.V; 1994.

[16] K. L. Reifsnider, *Fatigue of Composite Materials*. Netherlands: Elsevier Science B.V; 1991.

[17] E. F. Knott, J. F. Shaeffer and M. T. Tuley, *Radar Cross Section.* Boston: Artech House; 1993.

[18] M.C.Y. Niu, *Composite Airframe Structures*. Hong Kong: Conmilit Press Limited; 1992.

[19] F.C. Campbell, *Manufacturing Technology for Aerospace Structural Materials.* Elsevier Ltd; 2006.

[20] "GPS IR Satellite." Image from Space Command Website, n. pag. http://www.afspc.af.mil

Vita

Captain Javier Rodriguez graduated from Blanca Malaret High School in Sabana Grande, Puerto Rico in 1997. He entered undergraduate studies at the University of Puerto Rico, Mayaguez Campus (also known as “Colegio de Agrimensura y Artes Mecanicas”), where he graduated with a Bachelor in Mechanical Engineering in May 2003. In June 2003 he was commissioned as a second lieutenant through the Detachment 756 Air Force Reserve Officer Training Corps (AFROTC) at the University of Puerto Rico, Mayaguez Campus.

His first assignment was at the Warner Robins Air Logistics Center located in Warner Robins Air Force Base in Georgia. During his time at WRALC he served as a C-17 & C-5 structural engineer during his first three years. During his last year at the ALC he served as a Lead Fighter Bomb Rack Engineer. During his entire time at the ALC he also served as C-5 Aircraft Battle Damage Repair Engineer.

In August 2007 he entered The Graduate School of Engineering and Management at the Air Force Institute of Technology in Wright-Patterson Air Force Base, Ohio. Upon graduation, he will be assigned to the Materials and Manufacturing Directorate of the Air Force in Wright-Patterson Air Force Base, Ohio.

REPORT DOCUMENTATION PAGE		Form Approved OMB No. 0704–0188

1. REPORT DATE (DD–MM–YYYY)	2. REPORT TYPE	3. DATES COVERED (From — To)
26-03-2009	Master's Thesis	August 2007 — March 2009

4. TITLE AND SUBTITLE	5a. CONTRACT NUMBER
Fatigue Evaluation of Nanocomposites as Lightweight Electronic Enclosures for Satellites' Applications	5b. GRANT NUMBER
	5c. PROGRAM ELEMENT NUMBER
6. AUTHOR(S) Javier Rodriguez, Captain, USAF	5d. PROJECT NUMBER
	5e. TASK NUMBER
	5f. WORK UNIT NUMBER
7. PERFORMING ORGANIZATION NAME(S) AND ADDRESS(ES) Air Force Institute of Technology Graduate School of Engineering and Management (AFIT/EN) 2950 Hobson Way WPAFB OH 45433-7765	8. PERFORMING ORGANIZATION REPORT NUMBER AFIT/GMS/ENY/09-M03
9. SPONSORING / MONITORING AGENCY NAME(S) AND ADDRESS(ES) Intentionally Left Blank	10. SPONSOR/MONITOR'S ACRONYM(S)
	11. SPONSOR/MONITOR'S REPORT NUMBER(S)

12. DISTRIBUTION / AVAILABILITY STATEMENT

APPROVED FOR PUBLIC RELEASE; DISTRIBUTION UNLIMITED

13. SUPPLEMENTARY NOTES

14. ABSTRACT

Existing nanocomposite materials used for satellite applications don't offer the required conductivity and electromagnetic shielding protection, requiring metal shields in order to survive in space. The AFRL Materials and Manufacturing Directorate in conjunction with the private sector have developed a material that promises to blend the attributes of nanocomposites and metal materials. The M55J/RS3 material consists of carbon fibers combined with a polyisocyanate matrix, in which nickel nanostrands™ are added. The research effort investigated the changes in the EMI and ESD of the material after being subjected to cyclic loads. Four configurations of a symmetric layup with fibers oriented at 0/90/45/-45 degrees were evaluated. Three of the four configurations (midplane, exterior, and interlaminar) had nickel nanostrands™ added in different locations of the material. The exterior configuration had the best performance for resistance and EMI measurements for all stress levels. Evaluations of tested specimens showed that nickel nanostrands™ were undamaged during the test.

15. SUBJECT TERMS

Nanocomposites, Space, Cyclic Loads, Satellite Applications, Nickel Nanostrands™, Conductivity, Electromagnetic Interference, Electrostatic Discharge.

16. SECURITY CLASSIFICATION OF:			17. LIMITATION OF ABSTRACT	18. NUMBER OF PAGES	19a. NAME OF RESPONSIBLE PERSON
a. REPORT	b. ABSTRACT	c. THIS PAGE			Shankar Mall, Ph.D.
U	U	U	UU	104	19b. TELEPHONE NUMBER (Include Area Code) (937) 255-3636, ext 4587; e-mail: Shankar.Mall@afit.edu